UHASSELT
KNOWLEDGE IN ACTION

Maastricht University

Faculty of Medicine and Life Sciences
School for Life Sciences
Master of Biomedical Sciences

Master's thesis

The effect of EAAT3 modulation in oligodendroglial cells

Berra Ozcan

Thesis presented in fulfillment of the requirements for the degree of Master of Biomedical Sciences, specialization Molecular Mechanisms in Health and Disease

SUPERVISOR :

Prof. dr. Tim VANMIERLO

MENTOR :

Mevrouw Lieve VAN VEGGEL

2022
2023

Transnational University Limburg is a unique collaboration of two universities in two countries: the University of Hasselt and Maastricht University.

UHASSELT
KNOWLEDGE IN ACTION

www.uhasselt.be
Universiteit Hasselt
Campus Hasselt:
Martelarenlaan 42 | 3500 Hasselt
Campus Diepenbeek:
Agoralaan Gebouw D | 3590 Diepenbeek

UHASSELT
KNOWLEDGE IN ACTION

Maastricht University

Faculty of Medicine and Life Sciences
School for Life Sciences
Master of Biomedical Sciences

Master's thesis

The effect of EAAT3 modulation in oligodendroglial cells

Berra Ozcan

Thesis presented in fulfillment of the requirements for the degree of Master of Biomedical Sciences, specialization Molecular Mechanisms in Health and Disease

SUPERVISOR :

Prof. dr. Tim VANMIERLO

MENTOR :

Mevrouw Lieve VAN VEGGEL

The effect of EAAT3 modulation in oligodendroglial cells*

Berra Ozcan[1], Lieve van Veggel[1], and Tim Vanmierlo[1]

[1]Neuroscience research group, Biomedical Research Institute, Universiteit Hasselt, Campus Diepenbeek,
Agoralaan Gebouw C - B-3590 Diepenbeek

*Running title: *EAAT3 modulation in oligodendrocytes*

To whom correspondence should be addressed: Tim Vanmierlo, Tel: +32 (11) 26 92 28; Email: tim.vanmierlo@uhasselt.be

Keywords: EAAT3, modulation, oligodendroglial cells, HOG, glutathione

ABSTRACT

Oligodendrocyte dysfunction and demyelination are known to be contributing factors to neurodegenerative diseases such as multiple sclerosis (MS). Due to high levels of oxidative stress in the brain, oligodendroglial cells fail to conserve themselves and counteract myelin damage. Several studies have described the importance of the sodium-dependent excitatory glutamate transporter three (EAAT3) on the surface of oligodendroglial cells. It is hypothesized that increased levels of oxidative stress overwhelm the activity of EAAT3, resulting in a decreased glutathione (GSH) synthesis. However, little is known about the mechanism of GSH as a protective antioxidant, and research on EAAT3 modulation has been lacking. This study shows that modulating EAAT3 affects oligodendroglial cells *in vivo* and *in vitro*. First, we demonstrated that oligodendroglial cells can be targeted by bilateral intracerebroventricular injections of adeno-associated virus (AAV) serotype 2.9 *in vivo* in mice. Next, we showed that intracellular GSH increases in EAAT3 overexpressing human oligodendroglioma cells *in vitro* by GSH-NEM immunofluorescent staining. We further identified the effect of an EAAT3-specific inhibitor on EAE mice *in vivo*. Our data shed light on the function of EAAT3 in intracellular GSH synthesis and its protective effect in oligodendroglial cells. Together, they may lead to the reestablishment of differentiation, maturation, and survival of oligodendrocytes in neurodegenerative diseases.

INTRODUCTION

Recent epidemiological data from The Atlas of Multiple Sclerosis (MS) has shown that the number of people affected by MS since 2013 has increased from 2.3 million to 2.8 million. This means that every couple of minutes, someone in the world is diagnosed with MS. In Europe alone, the annual MS incidence is estimated at around 133 per 100,000 or approximately 1.2 million people in total, which is the highest number of all continents [1]. MS is most common in young adults around the age of 20-30 years old, with a male-to-female ratio of 1:2 [2]. The etiology of MS is not yet known; however, data suggests it might be due to an influence of genetic and environmental factors. Genetic factors include the association with genes such as the human leukocyte antigen class 2 (HLA2) or differences in hormonal levels. Environmental risk factors include obesity, smoking, an Epstein-Barr Virus (EBV) infection, or vitamin D deficiency. Symptoms can vary from fatigue, dizziness, blurred vision, and weakening of the limbs, eventually leading to death. Depending on the clinical subtype of MS, the symptoms can be present intermittently or progress over time. There are three main clinical subtypes, namely relapsing-remitting MS (RRMS), primary progressive MS (PPMS), and secondary progressive MS (SPMS). Most patients are diagnosed with RRMS, where symptoms appear in episodes that worsen over a few days, weeks, or months. After a while, symptoms will improve, only to occur again repeatedly. In PPMS, it takes years for symptoms to accumulate without periods of remission. In people with SPMS, RRMS gradually develops into PPMS over 10-15 years. Since there is no cure for MS, treatments only focus on targeting symptoms [3].

Physiologically, MS is a chronic, auto-immune disease affecting the central nervous system (CNS), which is caused by the activation of autoreactive T helper 1 (Th1), Th17, and CD8+ T cells against the myelin proteins that form the insulating myelin sheath around axons. When activated T cells enter the CNS via the blood-brain barrier (BBB), pro-inflammatory cytokines are released, creating an inflammatory environment. This environment further damages myelinating oligodendrocytes enwrapping neuronal axons. Moreover, it causes further breakdown of the BBB, which results in more transendothelial migration of activated T-cells, B-cells, and macrophages. While B-cells produce antibodies against myelin, macrophages engulf impaired oligodendrocytes, resulting in the demyelination of neuronal axons. In the early stages of MS, the damage is limited, making it possible for oligodendrocytes to heal and restart remyelination. However, in later stages, when levels of oxidative stress are too high, oligodendrocytes become irreversibly damaged, remyelination stops; and this results in permanent axonal loss and neurodegeneration [3, 4].

As mentioned before, one of the main hallmarks of MS pathology is chronic inflammation causing oxidative stress in the CNS, eventually leading to oligodendroglial and axonal death. Not only does oxidative stress affect existing oligodendrocytes; it also affects oligodendrocyte precursor cells (OPCs)[5]. OPCs are predecessors of mature myelinating oligodendrocytes and are abundant in the white and grey matter of the CNS. Immature OPCs highly express transcription factors Sox5, Sox6, Inhibitor of Differentiation 2 (Id2), and Id4. During differentiation towards myelinating oligodendrocytes, expression levels of these factors decrease; meanwhile, expression of genes such as myelin basic protein (MBP), myelin-associated glycoprotein (MAG), and myelin oligodendrocyte glycoprotein (MOG) increases. Additionally, oligodendrocyte transcription factor 1 (Olig1), Olig2, and Sox10 are genes expressed throughout the entire oligodendroglial lineage [6]. Together, this is a dynamic process orchestrated by epigenetic changes such as histone modifications and DNA methylation [7].

In response to oxidative stress and inflammation in the microenvironment, OPCs can migrate and differentiate into mature oligodendrocytes and replace damaged oligodendrocytes [7, 8]. However, in MS, the high inflammation and oxidative stress levels hinder OPCs from differentiating and halt the remyelination capability of oligodendrocytes [8, 9].

Several studies have already reported the effect of glutamate transport via excitatory amino acid transporters (EAATs) on OPC differentiation [5, 10-12]. EAATs are encoded by the solute carrier gene (SLC) and are mainly expressed in neurons. Glutamate transport happens via the cotransport of 3 Na^+ ions and 1 H^+ and the export of 1 K^+ ion. Currently, the five known EAAT isoforms (EAAT1-5) are known to transport glutamate to counter-balance the effects of glutamate excitotoxicity in neurodegenerative diseases [13]. Studies from Zhang et al. and Watts et al. have described the EAAT3 subtype to be expressed in the oligodendroglial lineage and also function as the only EAAT to transport cysteine [14, 15]. This means that cysteine, a key amino acid needed to synthesize glutathione (GSH), is transported via EAAT3. GSH is an abundant non-protein thiol formed intracellularly by linking cysteine, glycine, and glutamate [16]. Extensive research has characterized it by its antioxidant properties [17]. Recently, a review by Malik et al. described the function of EAATs during oxidative stress. When glutamate is released by neurons in the extracellular space of the CNS; glutamate is removed by specific EAATs on the surface of oligodendrocytes, neurons and astrocytes. In addition to glutamate, EAAT3 also transports cysteine in neurons and oligodendrocytes to produce GSH to serve as an antioxidant [18]. Next, a study from Escartin and colleagues stated that oxidative stress promotes the release of GSH by upregulating neuronal EAAT3 *in vitro* and *in vivo*. They found conserved antioxidant-responsive elements (AREs) in the promotor of the EAAT3 gene. AREs are involved in inducing expression of protective genes such as nuclear factor (erythroid-derived 2)-like 2 (Nrf2), under oxidative stress. Moreover, they showed that the induction of EAAT3 is a response to oxidative stress since EAAT3 and GSH levels rose significantly in neurons *in vivo* [19]. Similarly, it has been shown that oligodendrocyte and OPC functionality during oxidative stress was maintained via EAAT3 transport of cysteine for GSH synthesis [13, 20]. Studies also have demonstrated that the activity of EAAT3 is altered by changes in expression levels, changes in protein interaction, and recycling of EAATs. Several pathways, including the activation of protein kinase C, can regulate EAAT3 cycling from and to the cell

surface to increase or decrease EAAT3 expression at the membrane surface as a response to oxidative stress [21]. Additionally, a loss of EAAT3 results in a reduction of cysteine transport and GSH levels, which lead to an increased susceptibility to oxidative stress, as shown in previous studies [22-24]. This means that the cellular modulation of EAAT3 in neurons, astrocytes, and the oligodendroglial lineage functions as an oxidative stress response to maintain CNS homeostasis.

In conclusion, research suggests that increased levels of oxidative stress overwhelm EAAT3 activity in oligodendrocytes and their precursors, leading to less cysteine transport and lower GSH levels. It affects OPCs by impairing their maturation and differentiation ability, and affects oligodendrocytes by shutting down their remyelination ability [8]. Additionally, the modulation of EAAT3 on the surface of oligodendroglial cells to regulate cysteine transport might be able to increase GSH levels to exert protective effects. Delgado-Acevedo et al. already showed that GSH levels were increased in an obsessive-compulsive disorder (OCD) mouse model overexpressing EAAT3 [25]. In contrast to this, the effects of oxidative stress and EAAT3-mediated cysteine transport in oligodendroglial cells in the context of MS have been lacking. Therefore, to evaluate the consequences of EAAT3 modulation on intracellular GSH levels during oxidative stress, we used adeno-associated viruses (AAVs) *in vivo* and lentiviral vectors (LVs) *in vitro* to achieve targeted overexpression. Additionally, we tested the effect of 2-(furan-2-yl)-8-methyl-4-N-(2-methylphenyl) imidazo [1,2-A]pyridine-3-amine, an EAAT3 inhibitor, *in vivo* in mice.

EXPERIMENTAL PROCEDURES

Animal housing and study approval – All animal experiments were carried out in accordance with the European Communities Council Directive of 2010 (2010/63EU) and approved by the Ethical Committee for Animal Experimentation (ECAE) of Hasselt University (Limburg, Belgium). Female C57BL/6 mice (9-10 weeks old, Jackson Laboratories, ME, USA) weighing around 21-24 g, were acclimatized for 7 days and housed under a normal 12h light/dark cycle with free access to food and tap water.

Experimental auto-immune encephalomyelitis (EAE) – Female C57BL/6 mice received a subcutaneous injection with an emulsion containing 1 mg/ml myelin oligodendrocyte glycoprotein 35-55 (MOG_{35-55}) in complete Freund's adjuvant (CFA) and received two intraperitoneal injections of 70 ng pertussis toxin (PTX) (directly after MOG_{35-55} injection and 24 hours thereafter) (Hooke Laboratories, MA, USA). Mice were weighted and clinically scored (blinded) every day using a 5-point scale (0: no symptoms; 1: limp tail; 2: hind limp weakness; 3: complete hind limp paralysis; 4: complete hind limp paralysis and partial front leg paralysis; 5: death). Animals were sacrificed 21 days after immunization (n=15/group) by a lethal Dolethal injection (200 mg/kg, Vetoquinol, Northhamptonshire, UK), followed by a transcardial perfusion.

EAAT3 Inhibitor (2-(furan-2-yl)-8-methyl-4-N-(2-methylphenyl) imidazo [1,2-A]pyridine-3-amine) and Riluzole treatment – Female C57BL/6 mice were randomly allocated to the following groups: Group 1 no EAE induction + vehicle (n=18); Group 2 EAE induction + vehicle (n=18); Group 3 EAE induction + Riluzole (4mg/kg, Cayman, MI, USA)(n=18), Group 4 EAE induction + inhibitor (30 mg/kg, Chemspace, NJ, USA)(n=18). All mice were subcutaneously injected 2 times a day (min. 6 hours between both injections). Mice received 10 µl/g compound each time of injection for 21 days. Compounds were prepared one to three days prior of injections. Riluzole and inhibitor were first dissolved in 0,5% dimethyl sulfoxide (DMSO, Sigma-Aldrich, MO, USA). Afterwards, compounds were dissolved in 2% Tween 80 VWR, Leuven, Belgium) before dissolving it in 0,5% methylcellulose (Sigma-Aldrich, MO, USA). 0,5% DMSO without compound was used as a vehicle.

After treatment with vehicle, Riluzole and EAAT3 inhibitor for 20 days, mice were again injected with vehicle or inhibitor 30 minutes before sacrifice. Brains were collected and snap frozen in liquid nitrogen. Next, brains were crushed and collected in acetonitrile (Merck, NJ, USA) overnight. Crushed brains were centrifuged at 4000g at 4°C and the supernatant was collected for LC-MS measurement. The standard solution was made using 1 mg/ml, 100 µg/ml, 10 µg/ml, 1 µg/ml, 100 ng/ml, 10 ng/ml, 1 ng/ml, 100 pg/ml, 10 pg/ml, 1 pg/ml EAAT3 inhibitor dissolved in acetonitrile. For LC-MS measurements, the Shimadzu system equipped with a Shimadzu Nexera HPLC solvent delivery system (LC-40Dx3) with photo-diode array detector (SPD-M40) and a single quadrupole mass spectrometer (LCMS 2020) was used. The MS was attributed

with electron spray ionization (ESI). Chromatographic separation was achieved on an Shim-pack GIST C18-AQHP 1,9 mm column (2,1 mm x 100 mm) at a flow rate of 0,4 mL/min, an oven temperature of 40°C and an injection volume of 1 µl. A solvent gradient was applied starting from 95:5 water: acetonitrile for 2 min. Then ,the composition was linearly changed over the course of 6 minutes to a 5;95 water: acetonitrile mixture. The total run time was 11 minutes. Both solvents consisted of 0,1% formic acid.

Visual evoked potentials (VEPs) – Visual evoked potentials (VEPs) were measured before EAE induction (baseline) and pre-onset. Animals were adapted to the dark 12 hours prior to the start of the measurement. Potential light sources were covered with infrared filters. First, mice were anesthetized by 10 µl/g intraperitoneal injection with 20 mg/kg xylazine and 80 mg/kg ketamine. Next, dilatation of pupils was achieved by using 5 mg/ml Tropicol (Théa, Clermont-Ferrand, France) for 5 minutes and 15% phenylephrine (Théa, Clermont-Ferrand, France) for 2 minutes. A ground electrode was inserted in the base of the tail, a reference electrode in the tongue and an active electrode between the ears. Mice were placed on a heating pad at 38°C. Afterwards, 2 mg/g Vidisic (Bausch+Lomb, Laval, Canada) was used for the eyes to prevent them from drying out before the flash electrodes were placed on both eyes. The eyes were stimulated with 100 light flashes per eye.

Human oligodendroglioma (HOG) cell culture – Human oligodendroglioma cells (HOG) were gifted by Niels Hellings and grown to approximately 80% confluence in an uncoated T75 flask suited for sensitive/difficult adherent cells. Cells were maintained in Dulbecco's modified eagle medium supplemented with 1% Penicillin-Streptomycin (P/S, Sigma-Aldrich, MO, USA) and 10% heat-inactivated fetal calf serum (FCS, Biowest, Nuaillé, France) at 37°C and 5% CO_2. Cells were maintained in differentiation medium which is Dulbecco's modified eagle medium (Dmem 1X, Gibco, MA, USA) supplemented with 5 µg/ml Transferrin (Sigma-Aldrich, MO, USA), 5 µg/ml insulin from bovine pancreas (Sigma-Aldrich, MO, USA), 0,03 nM sodium-selenite (Sigma-Aldrich, MO, USA), 30 nM L-Thyroxine sodium salt pentahydrate (T3, Sigma-Aldrich, MO, USA), 1% Penicillin-Streptomycin (P/S, Sigma-Aldrich, MO, USA) and 0,05% heat-inactivated fetal calf serum (FCS, Biowest, Nuaillé, France) at 37°C in an atmosphere of 5% CO_2.

Glutathione (GSH) fluorescent immunohistochemistry – Animals were sacrificed by a lethal Dolethal injection (200 mg/kg, Vetoquinol, Northamptonshire, UK), followed by a transcardial perfusion. Brains were collected from each animal and immersed in 4% paraformaldehyde (PFA, P6148, Sigma-Aldrich, MO, USA) and 10 mM N-ethylmaleimide (NEM, Sigma-Aldrich, MO, USA) at 4°C overnight. Afterwards, brains were incubated in a sucrose gradient of 20% for 48 hours for cryoprotection and sectioned at 10 µm thickness (Leica CM3050S, Wetzlar, Germany). Cryosections were dried and incubated in acetone for 10 minutes and washed with 0,05% PBS-Tween. Non-specific background signal was blocked by incubating cryosections for 30 minutes in 10% diluted protein block (Dako, Glostrup, Denmark) in PBS. After blocking, sections were preincubated with 10 mM N-ethylmaleimide (NEM, Sigma-Aldrich, MO, USA) for 1 hour at 4°C. Cryosections were incubated overnight at 4°C with mouse anti-GSH-NEM (1/100, MAB3194, clone8.1GSH, Milipore, MA USA) and anti-Olig2 (1/500, AF2418, R&D systems, MN, USA). Unattached primary antibodies were washed off with PBS and incubated for 1 hour at room temperature with secondary antibodies Alexafluor 488 goat anti-mouse IgG (1/600, Invitrogen, MA, USA) and Alexafluor 555 donkey anti-goat IgG (1/600, Invitrogen, MA, USA). Counterstaining of nuclei was done with DAPI (Invitrogen, MA, USA) for 10 minutes at room temperature. Cryosections were washed with PBS and mounted with fluorescent mounting medium (DAKO, Glostrup, Denmark). Images of the corpus callosum and left/right ventricles were taken using confocal microscopy (Carl Zeiss LSM 880 AiryscanFAST, Jena, Germany) and visualized with the Fiji ImageJ software.
Details of primary antibodies are shown in Table S1.

Statistical analysis – Statistical analysis was performed using GraphPad Prism 9 software (GraphPad software Inc, CA, USA). Outliers were selected and excluded based on Dixon with a significance level of 0,05. Normality was tested using the Shapiro-Wilk test for normality. Normally distributed data were analyzed using a One-way ANOVA with Tukey's or Dunnett's multiple comparison tests. All data are displayed as mean±SEM. *$p \leq 0,05$, **$p \leq 0,001$, ***$p \leq 0,0001$, ****$p < 0,0001$.

RESULTS

Intracerebroventricular injection of AAV2.9 shows more spreading throughout the brain in mice in vivo – To investigate whether the virus targeted the oligodendroglial cells, AAV-mediated green fluorescent protein (GFP) expression was initially examined in the brains of Sox10Cre and wild-type mice by immunofluorescent analysis. To obtain a widespread expression throughout different brain regions, we opted for a bilateral intracerebroventricular injection or an injection in the corpus callosum (CC) with AAVs of two different serotypes. AAV2.8 and AAV2.9 serotypes were chosen because it has been shown that they spread best in brain tissue [26-28].

Within the intracerebroventricular injection, we observed that the spreading of AAV2.9 was wider compared to AAV2.8. Serotype 2.9 showed GFP expression throughout the whole CC; serotype 2.8 remained local (Fig. 1A+B). Next, we further characterized differences between injection sites. The intracerebroventricular injection reached the complete CC, the parts of the ventricular walls, and reached into layers of the cortex. Meanwhile, an injection in the CC shows local spreading in the CC and the inner walls of the ventricles close to the injection site (Fig. 1A+C). Mice that received no injection show no fluorescent signal for GFP and Sox10-positive cells (Fig. 1D). Furthermore, we demonstrated the expression specificity of GFP in terms of the oligodendroglial cells. AAV2.9 reveals an overlay between GFP and Sox10 positive cells (Fig. 2A+B). Additionally, no difference is seen between AAV2.8 and AAV2.9 regarding the target specificity (Fig. 2A-D). Also, here, mice that received no injection show no fluorescent signal for GFP and Sox10 positive cells (Fig. 2E).

Heat-induced antigen retrieval and animal serum blocking enable fluorescent CC1 signal but not PDGFRα - To determine if the AAVs reached OPCs or only mature oligodendrocytes, we optimized an immunofluorescent staining for

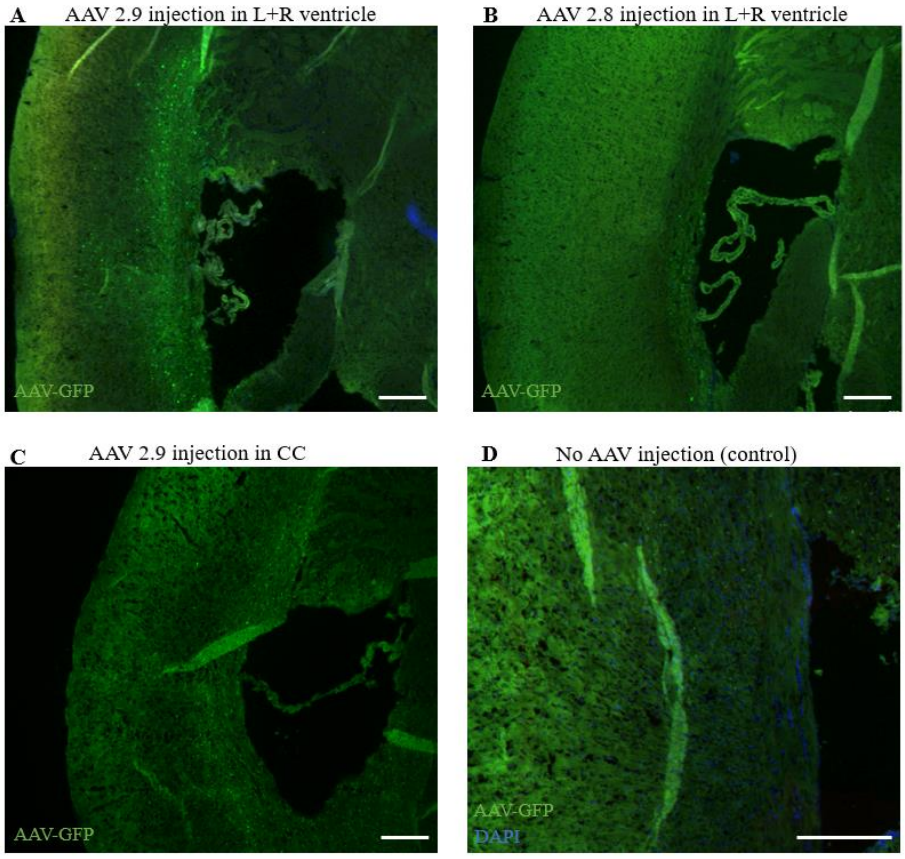

Fig. 1 –**AAV2.9 spreads better throughout the brain than AAV2.8. (A and B)** Immunofluorescent staining of an AAV2.9 and AAV2.8 (green) injection in the L+R ventricle of wild-type mice. **(C)** Immunohistochemical staining of an AAV2.9 injection in the CC of Sox10Cre mice. **(D)** Immunofluorescent staining of not injected Sox10Cre mice. All mice (n=2 per group) received 1 bilateral AAV injection (except control group). Six days after AAV injection, mice received one Tamoxifen injection during 3 days (except control group) and all mice were sacrificed seven days after the last Tamoxifen injection. AAV: adeno-associated virus, CC: corpus callosum, GFP: green fluorescent protein, L+R: left + right (Magnification; 10x, Scalebar; 250 µm)

PDGFRα and CC1 to differentiate between precursors and mature cells, respectively.

First, we stained for PDGFRα and CC1 without heat-induced antigen retrieval and a primary antibody dilution of 1/500 for PDGFRα and 1/50 for CC1 (Fig. S1). The GFP signal from the AAVs is not visible since it faded over time (Fig. S1A). No signal is detected for PDGFRα stained slices (Fig. S1C), but slices stained with CC1 show oligodendrocytes in the CC when the exposure increases (Fig S1D-E). The negative control shows no CC1-positive cells (Fig. S1F). To allow for the restoration of the tertiary structure of PDGFRα and CC1 and increase the access of primary antibodies to the epitopes of both antigens, we added an extra step by first performing heat-induced antigen retrieval. Heat-induced antigen retrieval reverses cross-links between antigens and can thereby lead to more visible signal in immunofluorescent staining. Furthermore, a dilution of 1/200 for PDGFRα was used. By employing this method, we visualized CC1 but not PDGFRα (Fig. S2B-E). Similar to Figure S1, no GFP signal is visible (Fig. S2A), and the negative control shows no CC1-positive cells (Fig. S2F). Since heat-induced antigen retrieval led to a more clear signal for CC1 but not for PDGFRα, we tried to block with

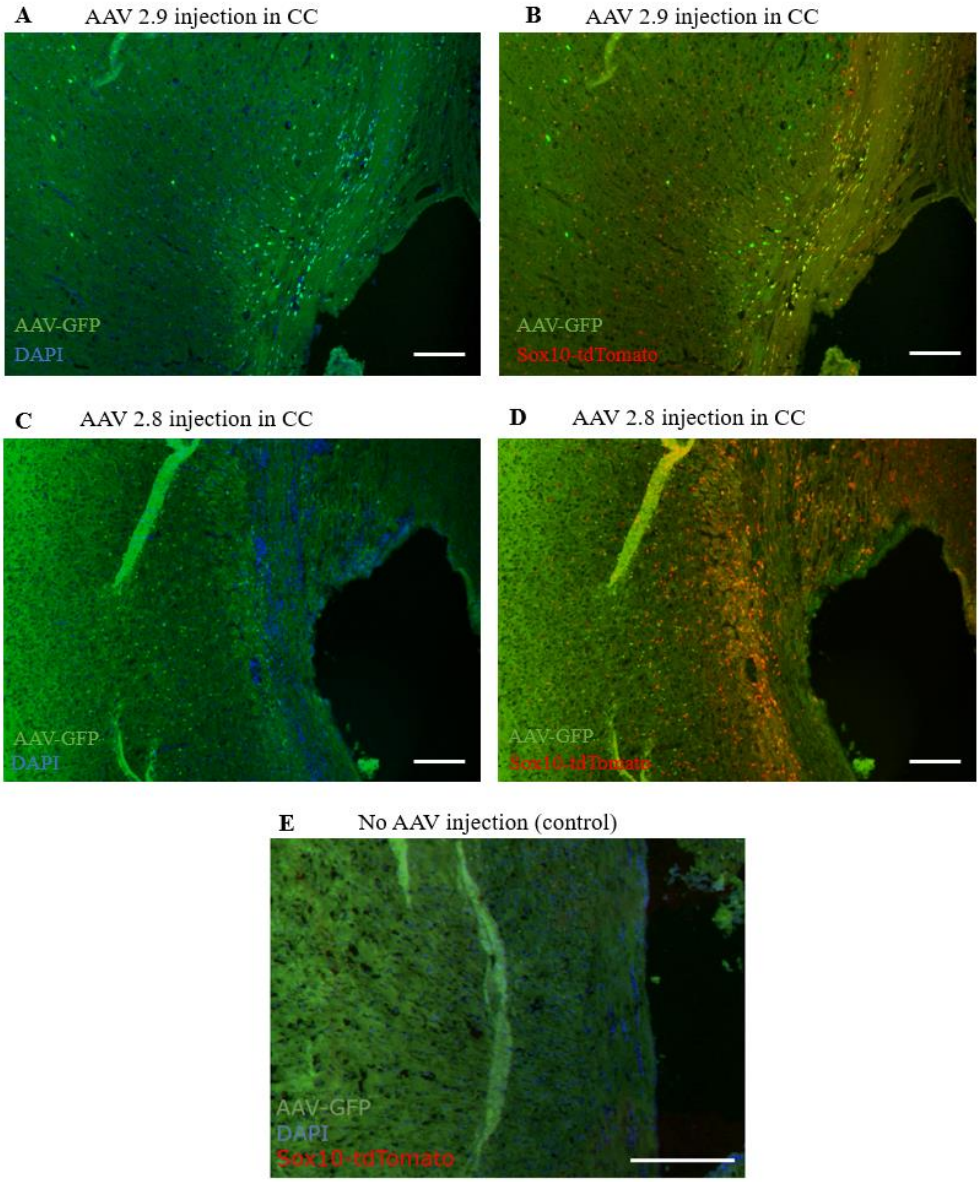

Fig. 2 – **AAV2.9 injected in the CC reaches oligodendroglial cells. (A+B)** Immunofluorescent staining of Sox10Cre mice which received an AAV2.9 injection in the corpus callosum. **(C+D)** Immunofluorescent staining of Sox10Cre mice which received an AAV2.8 injection in the corpus callosum. **(E)** Immunofluorescent staining of not injected Sox10Cre mice. All mice (n=2 per group) received 1 AAV injection (except control group). Six days after AAV injection, mice received 1 daily Tamoxifen injection for 3 days (except control group) and all mice were sacrificed 7 days after the last Tamoxifen injection. AAV: adeno-associated virus, CC: corpus callosum, GFP: green fluorescent protein (Magnification; 10x, Scalebar; 100 µm)

serum from the host species of the secondary antibodies (normal donkey serum and normal goat serum) in an attempt to visualize PDGFRα positive cells. Additionally, we used a dilution of 1/100 for PDGFRα. As mentioned previously, no GFP signal is visible since it faded over time (Fig. 3A). Interestingly, no PDGFRα signal could be seen even after blocking with animal serum and heat-induced antigen retrieval (Fig. 3C). On the other hand, the CC1 signal is more distinctly visible after the combination of heat-induced antigen retrieval and blocking with animal serum than with heat-induced antigen retrieval alone (Fig. 3D-E).

GSH-NEM staining of Olig2 positive cells can be visualized by confocal microscopy - To understand the effect of EAAT3 modulation on GSH synthesis of oligodendroglial cells, we first optimized an immunofluorescent staining to visualize GSH intracellularly. Here, we used mouse brains that were fixed in N-ethylmaleimide (NEM). NEM is a low molecular mass molecule with a high affinity against sulfhydryl groups found on GSH. Upon reaction with the sulfhydryl groups of GSH, its active form is locked in place to prevent GSH degradation. This results in the formation of GSH-NEM. We then used fluorescent immunohistochemistry

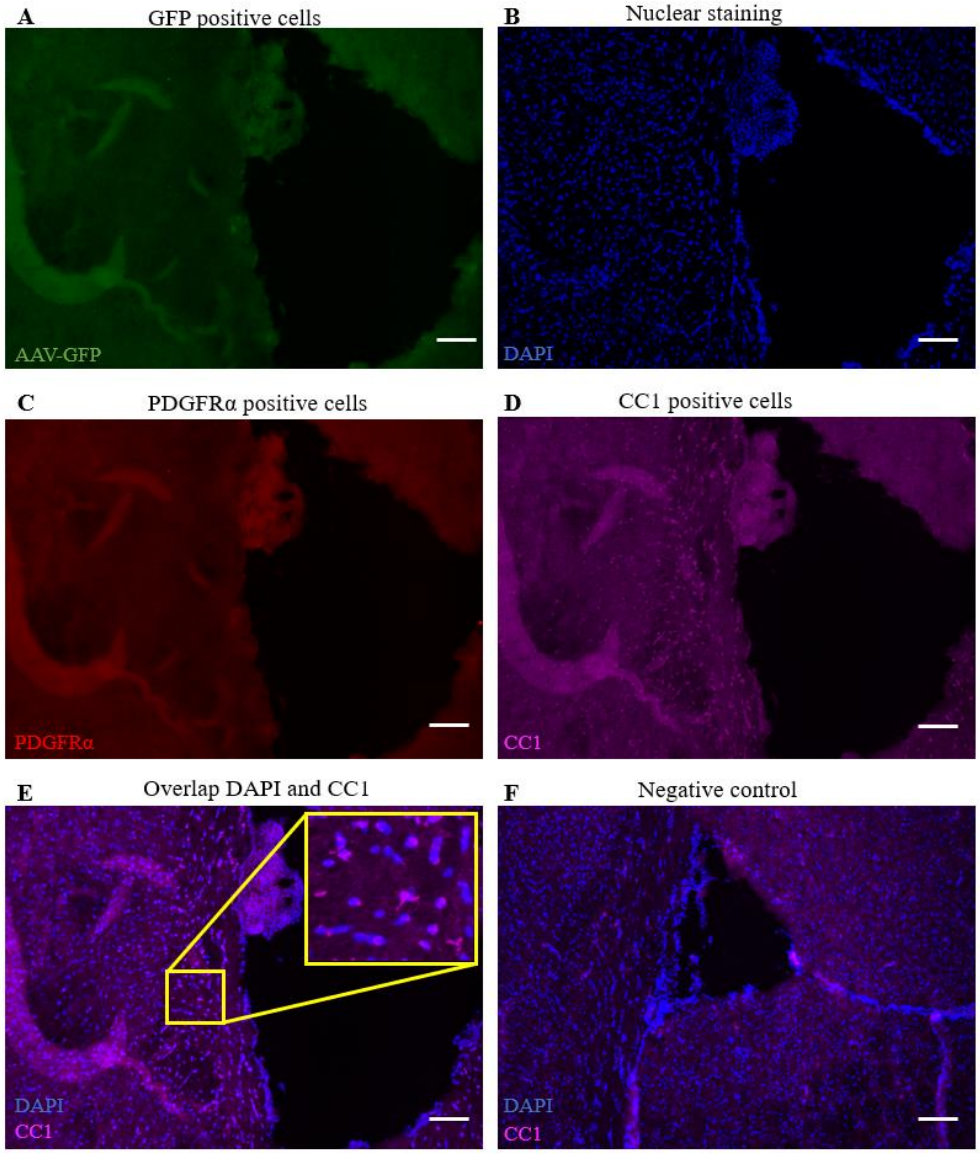

Fig. 3 – **Visualization of CC1 but not PDGFRα in mouse brain tissue after heat-induced antigen retrieval and blocking with 10% normal donkey and normal goat serum. (A-D)** Immunofluorescent staining of the CC using GFP, DAPI, PDGFRα (1/100, R&D systems) and CC1 (Calbiochem). GFP signal from AAVs are not visible since they have faded over time. **(E)** Overlap of DAPI and CC1 staining of the CC with 40x magnification (yellow box). **(F)** Negative control. CC: corpus callosum, CC1: anti-adenomatous polyposis coli clone 1, GFP: green fluorescent protein, PDGFRα: platelet-derived growth factor receptor alpha. (Magnification; 10x, Scalebar; 100 µm)

with an antibody specific to GSH-NEM to visualize intracellular GSH levels.

First, we implemented our standard staining protocol and incubated mouse brain slices for 1 or 4 hours in NEM to observe any differences between the two methods. Figure S3 shows mouse brain slices incubated for 4 hours in NEM. Here, cells are positive for GSH-NEM and Olig2 (Fig. S3A-C). The brain sample shows a cloudy structure with a weak fluorescent signal for GSH-NEM (Fig. S3A). However, the negative control also shows cloudy, slightly fluorescent structures (Fig. S3D). Colocalization of GSH-NEM and Olig2 or DAPI is not clearly visible (Fig. S3E-F). Following this, figure S4 shows mouse brain slices with an incubation time of 1 hour for NEM. Similar to figure S3, cells show a cloudy outline with weak fluorescent cells for GSH-NEM along the CC (Fig. S4A), and strong fluorescence for Olig2 (Fig. S4C). Also, here, no significant difference is seen between the GSH-NEM signal and the negative control (Fig. S4A+D). Overlapping images show a positive signal for GSH-NEM in Olig2-positive cells. Moreover, a clearly visible cell shape around the nucleus can be seen (Fig. S4E-F). However, the negative control also shows a GSH-NEM positive signal. In addition, no significant difference is seen between slices that were incubated for 1 and 4 hours. To reduce the background signal in the negative control, we used serum of the host species of the secondary antibodies as a blocking together with incubation of the slices in Sudan black. Again, slices were incubated in NEM for 1 and 4 hours. Cells in the CC are GSH-NEM and Olig2 positive (Fig. S5A-C). Interestingly, after serum blocking and incubation with Sudan black, the negative control is still positive for GSH-

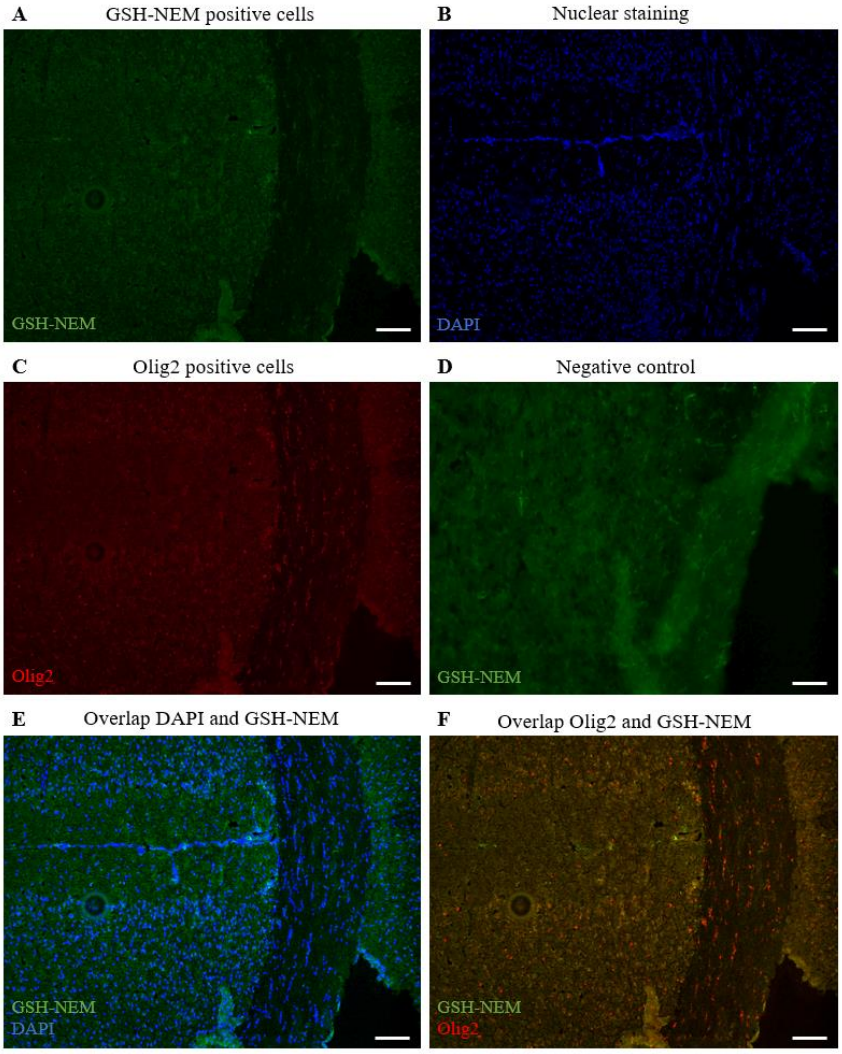

Fig. 4 – **Visualization of GSH-NEM in mouse brain tissue after blocking with 10% normal donkey and normal rabbit serum, Sudan black and 1 hour of NEM incubation. (A-C)** Immunofluorescent staining of mouse brain tissue (CC) using GSH-NEM, DAPI and Olig2. **(D)** Negative control. **(E)** Overlap of GSH-NEM and DAPI. **(F)** Overlap of GSH-NEM and Olig2. CC: corpus callosum, GSH-NEM: glutathione-N-ethylmaleimide, NEM: N-ethylmaleimide, Olig2: Oligodendrocyte transcription factor 2. (Magnification; 10x, Scalebar; 100 µm)

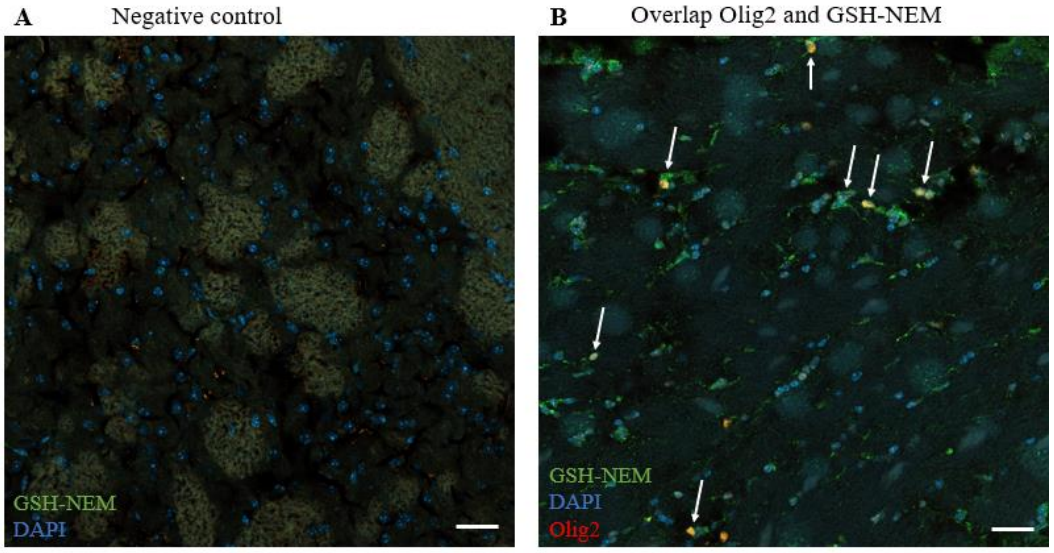

Fig. 5 – **Visualization of GSH-NEM in mouse brain tissue by confocal microscopy after blocking with 10% DAKO protein block and 1 hour of NEM incubation. (A)** Negative control. **(B)** Immunofluorescent staining of mouse brain tissue (CC) using GSH-NEM, DAPI and Olig2. Colocalization of GSH-NEM and Olig2 (white arrows). CC: corpus callosum, GSH-NEM: glutathione-N-ethylmaleimide, NEM: N-ethylmaleimide, Olig2: Oligodendrocyte transcription factor 2. (Magnification; 10x, Scalebar; 100 µm)

NEM (Fig. S5D). Again, here, GSH-NEM is visible in the cellular body of Olig2-positive cells (Fig. S5E-F). Equivalent to figure S5, cells in the CC show a positive signal for Olig2 and GSH-NEM (Fig. 4A-C). The latter is also seen in the negative control (Fig. 4D). Likewise, the colocalization of GSH-NEM is visible around Olig2-positive cells.

To detect a more prominent difference between the stained brain slices and the negative control, we chose to stain experimental auto-immune encephalomyelitis (EAE) and wild-type brain slices that were not fixed in NEM. In an attempt to eliminate the high background signal, we switched the fluorescent stainings for Olig2 and GSH-NEM from red to green and from green to red, respectively. Notably, cells in the CC show a positive signal for Olig2 and GSH-NEM in both the control (Fig. S6A-C) and stained samples (Fig. S6D-F). In EAE brain tissue, the stained samples show less signal for Olig2 and GSH-NEM (Fig. S7D-F) than the negative control (Fig. S7A-C).

Finally, we took brain samples of the first GSH-NEM staining (Fig. S3+S4) but visualized them by confocal microscopy. Confocal microscopy only illuminates a selected part of the slide instead of distributing light evenly throughout the whole sample. Moreover, confocal microscopy allows for the collection of multiple images throughout the different layers of the brain sample that can be stacked over each other to get a three-dimensional image. Together, this leads to a higher-quality image and a reduced background signal. The negative control shows green fluorescent areas in the brain sample. However, there is no fluorescence seen intracellularly since there is no clear fluorescent shape present that surrounds the nucleus (Fig. 5A). On the other hand, the stained sample shows a clear fluorescent GSH-NEM signal surrounding the cell nucleus (Fig. 5B).

EAAT3 overexpression increases GSH production in HOG cells - To see whether GSH content would be affected by EAAT3 overexpression, we performed a GSH-NEM staining on HOG cells that were transduced with a lentivirus containing an EAAT3 and GFP gene to generate EAAT3 overexpression. These cells will be referred to as HOG-EAAT3. HOG cells transduced with an empty vector only containing GFP, without the EAAT3 gene, are referred to as HOG-control and possess no EAAT3 overexpression. HOG-control and HOG-EAAT3 cells were treated with 0 mU and 3 mU glucose oxidase (GO) to induce oxidative stress. GO is an enzyme that catalyzes the oxidation of D-glucose to D-glucono-δ-lactone. This hydrolyzes further to D-gluconic acid and H_2O_2. The produced H_2O_2 creates oxidative stress in the cellular environment [29]. HOG-control cells treated with 0 mU GO show more GFP signal and are less round in shape compared to HOG-control cells treated with 3 mU GO (Fig. S8A+D). GSH content between both conditions is also different. HOG-control cells treated with 0 mU show more

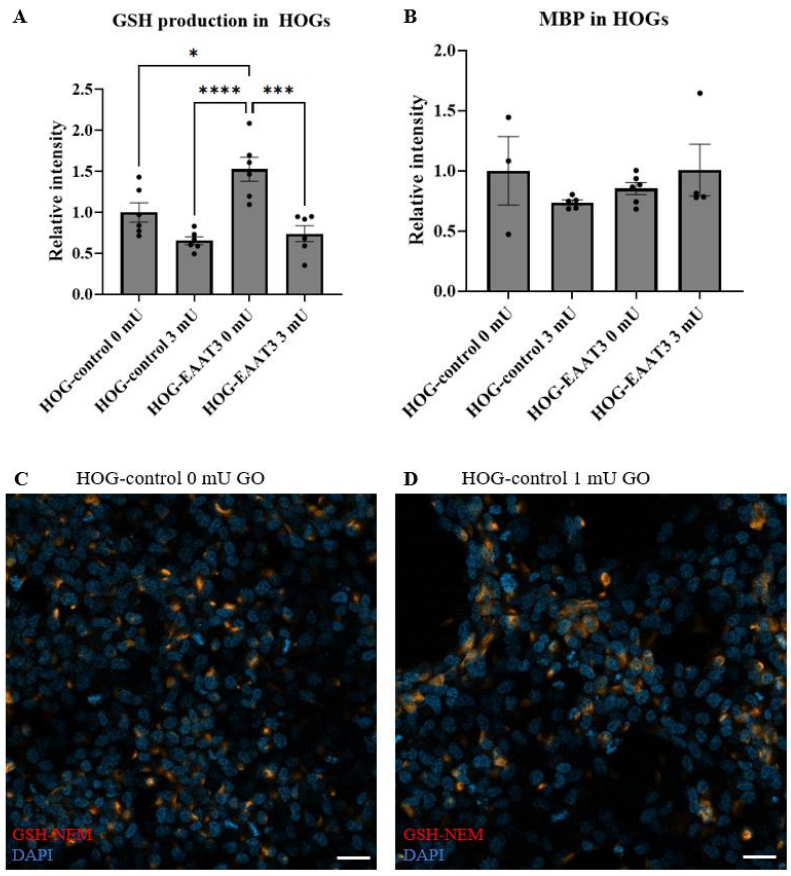

Fig. 6 – **GSH production in HOG-EAAT3 overexpressing cells increases significantly. Cells were treated at day 0 and 2 with 0 or 3 mU GO.** At day 4, cells were fixed and stained for GSH-NEM and MBP. **(A)** The relative GSH production in HOG-control and HOG-EAAT3 treated with 0 and 3 mU GO. **(B)** The relative MBP expression in HOG-control and HOG-EAAT3 cells treated with 0 and 3 mU GO. **(C)** Confocal image of HOG-control cells treated with 0 mU GO. **(D)** Confocal image of HOG-control cells treated with 1 mU GO. The relative intensity of GSH-NEM/GFP and MBP/GFP was calculated by the mean % area of the cells per well (n=6/group) and normalized to HOG-control 0 mU GO. Six pictures were taken per well. Data is depicted of 1 independent experiment. Data were analyzed using an ordinary one-way ANOVA with Tukey's multiple comparisons and are displayed as mean ± SEM (**p≤0,01, ***p≤0,0001, ****p<0,0001) (Magnification; 20x, Scalebar; 100 µm) EAAT3: excitatory amino acid transporter 3, GFP: green fluorescent protein, GO: glucose oxidase, GSH-NEM: glutathione-N-ethylmaleimide, HOG: human oligodendroglial cell, MBP: myelin basic protein, NEM: N-ethylmaleimide.

fluorescence throughout the whole cell body than HOG-control cells treated with 3 mU (Fig. S8B+E). DAPI signal is not different between both conditions. Similar to the previous figure, HOG-EAAT3 cells treated with 0 mU GO are less rounded and have a higher fluorescent signal for GSH-NEM than HOG-EAAT3 cells treated with 3 mU GO (Fig. S9A-F). After quantification of GSH content in both conditions, we show that GSH production in HOG-EAAT3 cells treated with 0 mU is significantly higher than in HOG-control cells treated with 0 mU. In addition to this, HOG-EAAT3 cells treated with 0 mU show a significantly higher GSH production when compared to HOG-control cells treated with 3 mU. Interestingly, HOG-EAAT3 cells treated with 3 mU have a significantly lower GSH content than the HOG-EAAT3 treated with 0 mU. Additionally, HOG-control and HOG-EAAT3 cells treated with 3 mU have similar relative intensities (Fig. 6A).

Next, we evaluated differentiation by measuring the relative intensity of MBP of these cells with the same conditions as mentioned above. We show no significant difference between the different cells and conditions. HOG-control cells treated with 0 mU and HOG-EAAT3 cells treated with 3 mU show similar intensities. HOG-control cells treated with 3 mU have a lower intensity when compared to HOG-control cells treated with 0 mU (Fig. 6B). Confocal images show a clear difference in GSH-content between HOG-control cells treated with 0 and 1 mU GO. The number HOG-control cells producing intracellular GSH is higher when cells are treated with 0 mU in comparison with one mU GO (Fig. 6C+D).

MBP mRNA expression is increased in HOG-EAAT3 cells – To determine the expression levels of myelination genes in HOG-control and HOG-EAAT3 cells treated with 0 mU and 3 mU GO, we performed a quantitative PCR. Additionally, to confirm EAAT3 overexpression in HOG-EAAT3 cells, we looked at SLC1A1 expression. The relative expression of MBP in 3 mU-treated HOG-control cells is lower in comparison with 0 mU-treated HOG-control cells (Fig. 7A). HOG-EAAT3 cells treated with 0 mU GO have a comparable relative MBP expression with HOG-control cells treated with 0 mU GO. HOG-EAAT3 cells treated with 3 mU show a lower relative MBP expression compared to HOG-EAAT3 treated with 0 mU GO. Figure 7B shows a significantly higher relative SLC1A1 expression of HOG-control cells treated with 0 mU compared to 3 mU-treated HOG-control cells. Furthermore, we see a significant difference between 0 mU-treated HOG-control and 3 mU-treated HOG-EAAT3 cells. Next, the relative Id2 expression of HOG-EAAT3 cells treated with 0 mU is significantly higher than HOG-control cells treated with 3 mU GO (Fig. 7C). Again, the relative Id2 expression of 3 mU-treated HOG-EAAT3 cells and 0 mU-treated HOG-control cells is similar to each other. Relative expression of SLC1A1 in untreated HOG-EAAT3 cells show a significant increase compared to HOG-control cells (Fig. 7D).

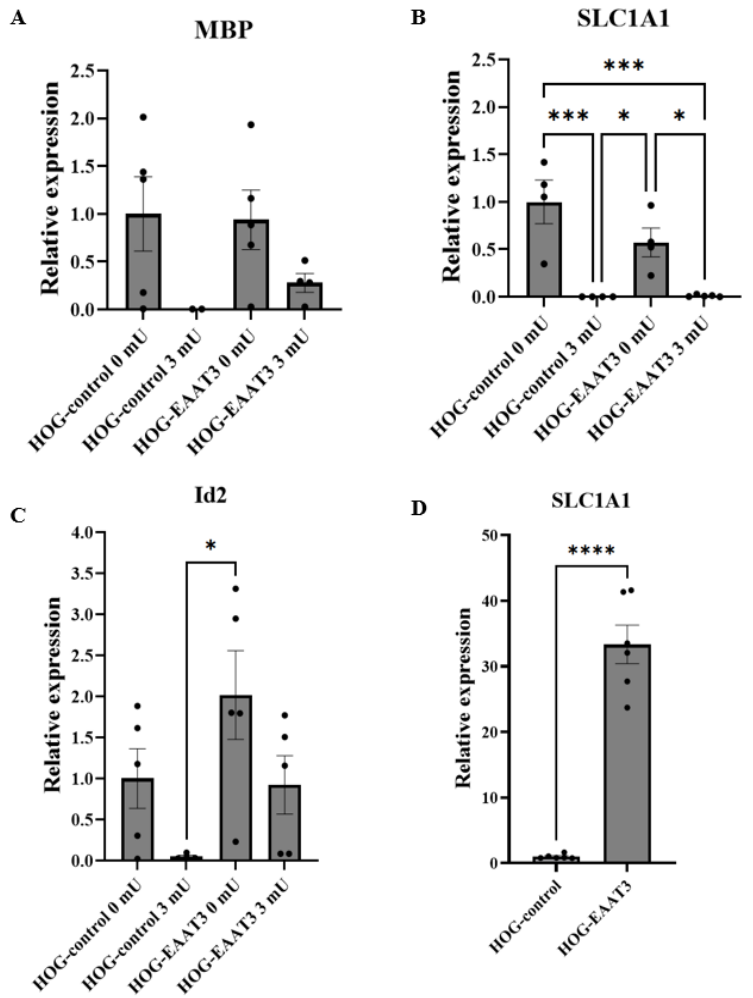

Fig. 7 – **mRNA expression of MBP is increased in HOG-EAAT3 cells treated with 0 mU GO.** Cells were treated at day 0 and 2 with 0 or 3 mU GO (n=6 wells/group). At day 4, cells were lysed for RNA isolation and cDNA synthesis. **(A)** MBP, **(B)** SLC1A1 and **(C)** Id2 expression in HOG-control cells and HOG-EAAT3 cells treated with 0 and 3 mU GO. **(D)** SLC1A1 expression in untreated HOG-control and HOG-EAAT3 cells. Data are corrected for the most stable housekeeping genes (YWHAZ and GAPDH for (A), (B) and (C) and CyCa and PGK for (D)) and normalized to HOG-control 0 mU. Data are from one independent experiment. Data were analyzed using an ordinary one-way ANOVA with Tukey's multiple comparisons for (A), (B) and (C), and an unpaired t-test for (D). Data are displayed as mean ± SEM (*p≤0,05; ***p≤0,0001; ****p<0,0001). EAAT3: excitatory amino acid transporter 3, GO: glucose oxidase, HOG: human oligodendroglial cell, Id2: Inhibitor of differentiation 2, MBP: myelin basic protein, SLC1A1: solute carrier 1A1

Injection of the EAAT3 inhibitor has an effect on EAE mice in vivo - To investigate whether EAAT3 modulation affects EAE, we subjected mice to EAE and treated them with 2-(furan-2-yl)-8-methyl-4-N-(2-methylphenyl) imidazo [1,2-A]pyridine-3-amine, an EAAT3 inhibitor. We compared visual evoked potentials (VEPs), weights, and EAE scores of mice which received, EAAT3 inhibitor (30 mg/kg), riluzole (4 mg/kg), or vehicle treatments.

Before EAE induction and at pre-onset of the disease, the VEPs of six mice from each group were measured to assess visual impairments in EAE mice. Baseline latency times are not significantly different between groups (Fig. 8A). At pre-onset, vehicle-treated EAE mice show a significantly longer latency than vehicle-treated non-EAE mice. Interestingly, EAE mice that are treated with EAAT3 inhibitor show significantly shorter latency when compared to the vehicle-treated EAE mice. Moreover, the latency of riluzole-treated EAE mice increases compared to vehicle-treated EAE mice (Fig. 8B). During the course of 20 days, we saw an increasing trend in the average weights of EAE mice treated with EAAT3 inhibitor and vehicle. Average weights of EAE mice treated with riluzole and non-EAE mice also show an increasing trend. However, this is lower than the other two groups (Fig. S10A). The average clinical scores during this period show that a few mice started to experience minor motor deficits on days 14-15 after immunization, which is less than expected in this

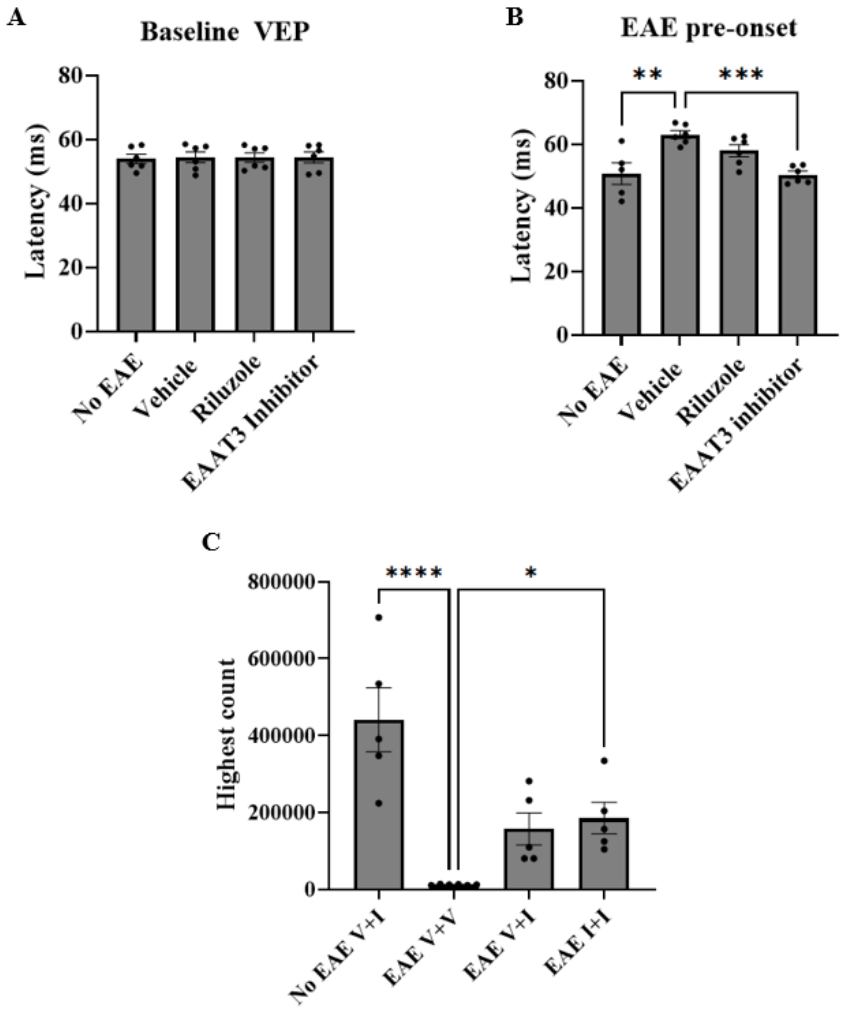

Fig. 8 – **EAAT3 inhibition affects visual evoked potentials in EAE mice at pre-EAE onset and concentration is highest 30 minutes after injection in non-EAE mice. (A)** Baseline visual evoked potentials latency times of mice before immunization and treatment (n=6/group). **(B)** Latency times of mice 5 days after immunization (pre-onset of EAE) and treatment (n=6/group). **(C)** LC-MS data of highest EAAT3 inhibitor count in brains of EAE mice (n=6/group). Data were analyzed using an ordinary one-way ANOVA with Tukey's multiple comparisons for (A) and (B) and Dunnett's multiple comparisons for (C). Data are displayed as mean ± SEM (*p≤0,05; **p≤0,001; ***p≤0,0001; ****p<0,0001). EAE: experimental autoimmune encephalomyelitis, I: inhibitor, LC-MS: liquid chromatography-mass spectrometry, V: vehicle, VEP: visual evoked potentials.

model. Furthermore, mice recovered from this in the following days (Fig. S10B).

After 20 days of treatment with vehicle, EAAT3 inhibitor and riluzole, mice received EAAT3 inhibitor or vehicle injections 30 minutes before sacrifice to see whether the EAAT3 inhibitor accumulated in the brain over time. Figure 8C shows liquid chromatography-mass spectrometry (LC-MS) data with the highest EAAT3 inhibitor count detected in the brains. EAE mice that previously received vehicle, and are injected with EAAT3 inhibitor before sacrifice (EAE V+I) show similar inhibitor counts compared to EAE mice that only received inhibitor injections (EAE I+I). Furthermore, the latter is significantly higher compared to the counts of EAE mice that only received vehicle (EAE V+V). Non-EAE mice that previously received vehicle, and are injected with EAAT3 inhibitor before sacrifice (No EAE V + I) have the highest count detected in the brain.

DISCUSSION

Bilateral intracerebroventricular AAV2.9 injections as a tool to induce EAAT3 overexpression in oligodendroglial cells in vivo – Failure of oligodendroglial cells has been reported in disorders such as MS, Alzheimer's disease, and Amyotrophic lateral sclerosis. Therefore, the main goal of this study was to gain insight into the effects of EAAT3 modulation on oligodendroglial cells and its impact on MS pathology to aim for possible innovative therapeutics on neurodegenerative diseases [30]. To reach oligodendroglial cells specifically, we opted for injecting AAV2.8 or AAV2.9 into the lateral ventricles or the CC. Evidence shows that the capsid protein determines the cellular tropism and transduction efficiency of AAVs [31]. Using the capsid protein of AAV serotype 8 and 9 and the genome of AAV serotype 2, AAV2.8 and AAV2.9 were engineered by Leuven Viral Vector Core. These vectors reportedly have an efficiency up to 5 to 100 fold higher in the brain compared to AAVs with capsid proteins of AAV serotype 1 or 2 [32]. Moreover, we used AAVs with a MAG promotor which previously showed a specificity of around 90% in oligodendrocytes of the rat striatum since it targets oligodendroglial cells expressing the MAG protein [33]. Comparable with a study of Peelaerts et al., our study showed that an injection of AAV2.9 showed more target specificity than AAV2.8. Furthermore, we show that an intracerebroventricular injection spreads wider throughout the brain compared to an injection in the CC. The advantage of the ventricles connecting other brain regions via cerebrospinal fluid flow is that it helps to reach the entire length of the CC and parts of the ventricular walls. An injection in the CC only allows for local spread [33]. Together, we suggest to deliver an intracerebroventricular injection of AAV2.9 for future experiments since it would achieve the highest target specificity and best expansion in the brain. Furthermore, this indicates that it is possible to achieve EAAT3 overexpression via AAV-mediated EAAT3 gene delivery to oligodendroglial cells specifically.

To specify if AAVs could also target OPCs, we optimized immunofluorescent stainings for PDGFRα and CC1. PDGFRα encodes for a transmembrane protein on the surface of OPCs. On the other hand, CC1 is used to target mature oligodendrocytes, despite being raised against the adenomatous polyposis coli (APC) protein, a protein involved in cell adhesion. Previous studies show that the CC1 antibody binds the highly-upregulated RNA-binding protein Quaking 7 in myelinating oligodendrocytes [34]. Our study shows that CC1 staining could be visualized with heat-induced antigen retrieval in combination with the use of animal serum as a blocking agent. Heat-induced antigen retrieval led to the recovery of cross-linked proteins in the tissue to ensure binding of the CC1 primary antibody. Furthermore, we reduced the background signal by using serum matching the secondary antibody species. This serum carries antibodies that bind to reactive sites in the tissue and prevents non-specific binding of the secondary antibody used in the staining [35]. Surprisingly, using both heat-induced antigen retrieval and animal serum blocking, PDGFRα could not be visualized. This might be due to the antibody not being suitable for immunofluorescence. Moreover, the manufacturer specifies that the antibody is validated for Western Blot, immunohistochemistry, and neutralization [36]. In contrast, Pagani and colleagues showed successful PDGFRα fluorescent stainings in murine hindlimb slices. Their method differed from ours in that they added 0,1% cold water fish skin gelatin, Triton X-100, and 300 mM glycine to the blocking buffer for 2 hours [37]. These components reduce non-specific binding, which might lead to a better fluorescent signal. Using these components together as a blocking buffer in future experiments can minimize the background signal, resulting in a clear fluorescent signal from

PDGFRα. We can also rule out that OPCs were not present in these slices due to the age of the mice (8-20 weeks old). Indeed, the OPC pool in the CNS does decline in an age-related manner; however, a certain amount of OPCs will always be present to support basic CNS homeostasis [38]. In conclusion, CC1 can be visualized by using heat-induced antigen retrieval and normal animal serum. We could not visualize PDGFRα but by using a different composition of the blocking buffer, a longer blocking time, or an antibody suitable for immunofluorescent stainings, it might be possible to detect PDGFRα in future experiments. This staining can be used to visualize the colocalization of AAVs with OPCs and oligodendrocytes to confirm AAV target specificity by optimizing this protocol.

Quantification of intracellular GSH – To quantify the GSH synthesis in oligodendroglial cells of mice brains, we optimized an immunofluorescent staining to visualize intracellular GSH. Our study shows that the colocalization of oligodendroglial cells and GSH-NEM in brain tissue can be visualized by confocal microscopy but not with fluorescence microscopy due to the high background signal. We demonstrated that switching fluorophores did not reduce the background signal, as well as using animal serum and Sudan black as a blocking agent. Additionally, we could not detect any significant differences between a 1 and 4-hour incubation with NEM prior to staining. Besides this, we did not see significant differences between PFA-NEM-fixated and PFA-fixated brain slices. Hence, we recommend using PFA-NEM as a fixative to prevent GSH from degrading since it has a very short half-life of 10 minutes [39]. This will ensure GSH-NEM detection. On the other hand, with confocal microscopy, the difference between the control and the GSH-NEM stained samples was significantly improved. In line with this, Miller et al. showed similar results by visualizing GSH-NEM in brain slices. Moreover, they showed colocalization of GSH-NEM and glial fibrillary acidic protein (GFAP), a marker for astrocytes. Surprisingly, they could visualize GSH-NEM by fluorescence microscopy by incubating the sections with primary antibodies for 24 hours at 4 °C and washing the sections for 2 hours in PBS [40]. Furthermore, a study by Won et al. [41] and Malik et al. [42] performed a GSH-NEM staining in brain slices to show colocalization of GSH-NEM with astrocytes and neurons, respectively. Similar to our results, they show colocalization by using confocal microscopy. Together, this indicates that the intracellular GSH content can be visualized in oligodendroglial cells in brain slices via confocal microscopy. This can be used in future experiments to quantify intracellular GSH in oligodendroglial cells and compare it with EAE brains, where oligodendroglial cells are expected to have a lower GSH content.

In advance, we quantified the GSH content after exposure to GO in HOG-control and HOG-EAAT3 transduced cells *in vitro*. We show that intracellular GSH production of HOG-EAAT3 cells increases significantly compared to HOG-control cells. Surprisingly, EAAT3 overexpression did not have a protective effect on the cells in the presence of oxidative stress. As mentioned in the section above, the GSH-NEM staining is mostly reported and quantified in brain slices, not cell cultures. To the best of our knowledge, we are the first to issue this staining on cell cultures. Until now, many studies have made use of glutathione detection kits such as the monochlorobimane (MCB)-assisted GSH detection kit [43-45]. For example, Ishkaeva et al. used human glioma-derived cell lines to improve the procedure for MCB-assisted GSH detection. This assay allows for the characterization of the redox status of a cell by utilizing a fluorescent MCB dye with a high affinity for GSH [46]. This method differs from ours since they use a kit that is only suitable for detecting GSH in cell cultures; meanwhile, the GSH-NEM staining can be performed on both brain slices and cell cultures. In addition, the anti-GSH-NEM antibody (clone8.1) is also validated for ELISA, flow cytometry and Western Blotting, which means that it applies to various techniques. Next, one would expect HOG cell differentiation (MBP) to align with GSH content. Contrastingly, our MBP staining showed the differentiation of HOG-control and HOG-EAAT3 cells with and without exposure to oxidative stress to be insignificantly different from each other. Similar to our findings, the study of De Kleijn and colleagues looked at oligodendrocyte functioning in HOG cells. They found an increase of MBP in mRNA expression of differentiated HOG cells compared to undifferentiated HOG cells but did not see this difference with immunofluorescent cytochemistry [47]. Additionally, Long et al. showed that HOG cell lines OG33 and OG35 failed to express MBP protein expression via immunocytochemistry.[48] In contrast to this, Tiane et al. did observe a difference in MBP on protein level in HOG cells which were transfected

with a construct to increase the epigenetic status of MBP [49]. Hence, our MBP and GSH-NEM results are opposing each other, this can be linked to the fact that there was a high background signal detected in the MBP staining. This might have led to inaccurate MBP quantification. To conclude, our study showed that intracellular GSH content in HOG-EAAT3 cells did not improve during oxidative stress, but is significantly increased in the absence of oxidative stress, indicating that EAAT3-mediated cysteine transport is involved in intracellular GSH production of cells *in vitro*.

EAAT3 overexpression affects MBP expression in vitro – Following this, we determined the MBP, Id2 and SLC1A1 expression in HOG-control and HOG-EAAT3 cells in the same conditions as mentioned above. Our results show that MBP mRNA expression in HOG-EAAT3 cells treated with 0 mU GO is comparable with HOG-control cells treated with 0 mU. These results also fall in line with our results on the GSH production in HOG cells. There, we showed that HOG-control and HOG-EAAT3 cells treated with 0 mU have comparable GSH content. Next, our results show that 3 mU-treated HOG-EAAT3 cells show a lower MBP mRNA expression compared to 0 mU-treated HOG-EAAT3. Again, these results fall in line with our results of the GSH immunofluorescent staining. There, 0 mU-treated HOG-EAAT3 cells have significantly higher GSH content compared to 3 mU-treated HOG-EAAT3 cells. We would expect similar results for the MBP protein expression however, contrastingly, our immunofluorescent MBP stainings show different results in comparison with the MBP mRNA expression. Our results from the MBP staining show MBP in all conditions to be comparable with each other. As mentioned before, the results of the MBP quantification might be inaccurate which means we cannot compare it with the MBP mRNA expression. Again, this suggests that EAAT3 overexpression does not lead to differentiation. Moreover, EAAT3 overexpression shows no protective effect on HOG cells in the presence of oxidative stress; however, the opposite is seen in the absence of oxidative stress. Surprisingly, Id2 mRNA expression in 0-mU treated HOG-EAAT3 cells is significantly higher than HOG-control cells treated with 3 mU GO. This is in contrast to the MBP mRNA expression where 0 mU-treated HOG-EAAT3 show an increase in expression. Surprisingly, SLC1A1 mRNA expression of HOG-control cells is also increased when compared to HOG-EAAT3 cells. This is unexpected since HOG-control cells do not posses EAAT3 overexpression. Moreover, our previous results show that the SLC1A1 mRNA expression of untreated HOG-EAAT3 cells is significantly higher than HOG-control cells. We suspect that expression levels of SLC1A1 are altered after HOG cells were thawed and seeded. It is also possible that GO and sodium acetate (vehicle used for 0 mU) treatment could have an effect on the SLC1A1 mRNA expression. Together, our study shows that EAAT3 overexpression leads to the preservation of MBP expression in HOG cells that were not exposed to oxidative stress.

The effect of a selective EAAT3 inhibitor on EAE mice in vivo – Next, we used an EAE mouse model to evaluate EAAT3 inhibition *in vivo*. Our results show that non-EAE mice have a significantly shorter latency than vehicle-treated EAE mice before EAE onset. This means that optic nerve damage is present before the onset of motor symptoms in EAE mice. Similar to our experiment, Marenna et al. conducted VEP measurements in EAE mice to characterize functional and structural visual damages in EAE mice at pre-motor onset. They showed a significant increase in latency in EAE mice compared to healthy controls [50]. Previously, a study from Castoldi et al. also showed shorter VEP latencies in a dark agouti rat model of EAE [51]. Although VEPs are useful translational biomarkers to detect changes in CNS potentials, few studies have used this technique in EAE mice at pre-onset to detect changes in the integrity of the visual pathways to the primary visual cortex. Moreover, most studies focus on measuring chronic changes in VEPs at 4 or 7 weeks after immunization [52, 53]. In fact, next to Marenna and colleagues, we are the first study to measure VEP latencies at pre-onset in EAE mice. Exceptionally, EAE mice receiving EAAT3 inhibitor injections show significantly shorter VEP latencies than vehicle-treated EAE mice at pre-onset. This inhibitor was first described by Wu et al. as the first selective inhibitor of EAAT3 [54]. In their study, they screened a library of various potential EAAT3 inhibitors and found that 2-(furan-2-yl)-8-methyl-4-N-(2-methylphenyl) imidazo [1,2-A]pyridine-3-amine had the highest preference for EAAT3 inhibition over other EAAT subtypes. Before conducting our experiment, we performed a pilot study to investigate whether the inhibitor was able to cross the BBB and reach the brain (data not shown).

Here, we tested intranasal and subcutaneous injections, as well as inhibitor concentrations of 0,3 mg/kg and 30 mg/kg. LC-MS data from the pilot study showed that the EAAT3 inhibitor is able to cross the BBB and reach the brain. Furthermore, data showed that an inhibitor concentration of 30 mg/kg and subcutaneous injections led to a higher concentration reaching the brain. This means we would expect EAAT3 specific inhibition in EAE mice. Inhibiting EAAT3 would further lead to the worsening of EAE, and result in a longer VEP latency than the vehicle group. Since there are no other studies performed using the EAAT3 inhibitor yet, we cannot compare our results with previous data. Adversely, EAE mice did not show motor deficits even after 20 days post-immunization. A few mice showed a clinical score of two but soon started to recover, which is why the experiment was finished prematurely. A possible explanation could be extracted from the study of Ohgoh and colleagues. Here, they investigated the mechanism of EAAT3 and other glutamate transporters in neurons of EAE Lewis rats. Interestingly, they describe that EAE induction caused a significant increase in EAAT3 protein and mRNA levels. Therefore, it is hypothesized that EAAT3 and other glutamate transporters are upregulated when extracellular glutamate is released from neurons [55]. This might act as a compensatory mechanism for oxidative stress and might explain why mice were recovering early. Besides this, several other factors in our experiment might have led to our unexpected results. First of all, due to unforeseen circumstances, the EAE immunization kit (Hooke) was stored improperly during transport, which might have resulted in the instability of the MOG_{35-55} emulsion, mycobacterium emulsion, and the pertussis toxin buffer [56]. Secondly, the recommended pertussis toxin dose is between 85 and 110 ng. Since our experiment focused on inhibiting EAAT3, we expected a fast and severe development of EAE in mice. Therefore, we opted for a lower dose of pertussis toxin to prevent mice from reaching humane endpoints. We used a dose of 70 ng, which might have been too low to induce EAE [56]. Thirdly, it is reported that stress prior to EAE development reduces EAE severity. More specifically, the stress of administering compounds during the first ten days post-immunization postpones disease onset and reduces disease severity [56]. Since we injected mice twice a day with either the EAAT3 inhibitor, riluzole, or vehicle, this might have had a significant impact on the stress levels of these mice and led to a lack of EAE development. Lastly, based on the data for the most optimal administration route from our pilot study, we opted for a subcutaneous injection in the neck. However, for EAE immunization, injecting MOG_{35-55} subcutaneously in the neck is also required. This led to the unfortunate event of injecting the compound at the site of the MOG_{35-55} emulsion, which resulted in MOG_{35-55} leakage and swelling of the neck due to possible accumulation of the injected compounds in this area. As a solution, we switched to a subcutaneous injection in the flank; however, this was disadvantageous since it might have led to a lower compound concentration reaching the brain.

To investigate this, we collected the brains of mice from this experiment. Additionally, 30 minutes before sacrifice, mice received a single vehicle injection or a single EAAT3 inhibitor injection to see the difference in accumulation of the inhibitor in the brain. Our study shows that the measured maximum peak height of the EAAT3 inhibitor in non-EAE mice that received the EAAT3 inhibitor injection 30 minutes after sacrifice is significantly higher than EAE mice that received vehicle. Moreover, our data show that EAE mice receiving both EAAT3 inhibitor for 20 days and 30 minutes before sacrifice show no significant differences in maximum peak height compared to EAE mice that received a single EAAT3 injection 30 minutes before sacrifice. This shows that the EAAT3 inhibitor did not accumulate in the brain after 20 days of treatment. Our unpredicted results can be elucidated by the fact that the compound did not adequately reach the brain due to the switch to subcutaneous injections in the flank and the fact that the injected compounds accumulated in the neck, causing leakage, as mentioned previously. Taken together, we show that 2-(furan-2-yl)-8-methyl-4-N-(2-methylphenyl) imidazo [1,2-A]pyridine-3-amine has an effect on mice before EAE onset and might have an impact in the CNS after EAE development. For future experiments in line with this, we firstly recommend to use a higher dose of pertussis toxin to ensure EAE development. Secondly, to prevent the reduction of EAE severity, animal stress levels should be maintained as low as possible. Thirdly, to avoid MOG_{35-55} and compound leakage, accumulation, and swelling of the neck, a different administration route for MOG_{35-55} injection should be chosen. Previously, Murugesan et al.

performed active immunization of EAE by MOG_{35-55} peptide injection in the left and right flank of female C57BL/6 mice [57]. This lead to EAE development as expected, which means it could serve as an alternative administration route for future experiments.

CONCLUSION

Collectively, our data show that EAAT3 modulation is possible via bilateral intracerebroventricular injections with AAV2.9 to gain EAAT3 overexpression in oligodendroglial cells and visualizable via an optimized CC1 staining. Furthermore, we optimized an immunofluorescent staining protocol to visualize intracellular GSH and show that intracellular GSH content is increased in EAAT3-overexpressing HOG cells *in vitro*. Thereby indicating that cysteine transport and intracellular GSH production of HOG cells *in vitro* is mediated by EAAT3. Additionally, we show that EAAT3 overexpression does have a protective effect on HOG cells without oxidative stress *in vitro*. Furthermore, we show that MBP expression is maintained in EAAT3 overexpressing HOG cells. Next, we show that 2-(furan-2-yl)-8-methyl-4-N-(2-methylphenyl) imidazo [1,2-A]pyridine-3-amine as a selective EAAT3 inhibitor has an effect in pre-EAE onset in mice *in vivo*. The optimalisation of various techniques in our study is a stepping stone for further research into the potential effects of EAAT3 modulation on oligodendroglial cells in neurodegenerative diseases.

REFERENCES

1. MS international federation 2020 [Available from: https://www.atlasofms.org/map/belgium/epidemiology/number-of-people-with-ms.
2. McGinley MP, Goldschmidt CH, Rae-Grant AD. Diagnosis and Treatment of Multiple Sclerosis: A Review. JAMA. 2021;325(8):765-79.
3. Yang JH, Rempe T, Whitmire N, Dunn-Pirio A, Graves JS. Therapeutic Advances in Multiple Sclerosis. Front Neurol. 2022;13:824926.
4. Huang WJ, Chen WW, Zhang X. Multiple sclerosis: Pathology, diagnosis and treatments. Exp Ther Med. 2017;13(6):3163-6.
5. Vallejo-Illarramendi A, Domercq M, Perez-Cerda F, Ravid R, Matute C. Increased expression and function of glutamate transporters in multiple sclerosis. Neurobiol Dis. 2006;21(1):154-64.
6. Emery B, Lu QR. Transcriptional and Epigenetic Regulation of Oligodendrocyte Development and Myelination in the Central Nervous System. Cold Spring Harb Perspect Biol. 2015;7(9):a020461.
7. Tiane A, Schepers M, Rombaut B, Hupperts R, Prickaerts J, Hellings N, et al. From OPC to Oligodendrocyte: An Epigenetic Journey. Cells. 2019;8(10).
8. Spaas J, van Veggel L, Schepers M, Tiane A, van Horssen J, Wilson DM, 3rd, et al. Oxidative stress and impaired oligodendrocyte precursor cell differentiation in neurological disorders. Cell Mol Life Sci. 2021;78(10):4615-37.
9. Rodgers JM, Robinson AP, Miller SD. Strategies for protecting oligodendrocytes and enhancing remyelination in multiple sclerosis. Discov Med. 2013;16(86):53-63.
10. Kolodziejczyk K, Saab AS, Nave KA, Attwell D. Why do oligodendrocyte lineage cells express glutamate receptors? F1000 Biol Rep. 2010;2:57.
11. Spitzer S, Volbracht K, Lundgaard I, Karadottir RT. Glutamate signalling: A multifaceted modulator of oligodendrocyte lineage cells in health and disease. Neuropharmacology. 2016;110(Pt B):574-85.
12. Bergles DE, Jabs R, Steinhauser C. Neuron-glia synapses in the brain. Brain Res Rev. 2010;63(1-2):130-7.
13. Bjorn-Yoshimoto WE, Underhill SM. The importance of the excitatory amino acid transporter 3 (EAAT3). Neurochem Int. 2016;98:4-18.
14. Zhang Y, Chen K, Sloan SA, Bennett ML, Scholze AR, O'Keeffe S, et al. An RNA-sequencing transcriptome and splicing database of glia, neurons, and vascular cells of the cerebral cortex. J Neurosci. 2014;34(36):11929-47.
15. Watts SD, Torres-Salazar D, Divito CB, Amara SG. Cysteine transport through excitatory amino acid transporter 3 (EAAT3). PLoS One. 2014;9(10):e109245.
16. Lu SC. Glutathione synthesis. Biochim Biophys Acta. 2013;1830(5):3143-53.
17. Carvalho AN, Lim JL, Nijland PG, Witte ME, Van Horssen J. Glutathione in multiple sclerosis: more than just an antioxidant? Mult Scler. 2014;20(11):1425-31.
18. Malik AR, Willnow TE. Excitatory Amino Acid Transporters in Physiology and Disorders of the Central Nervous System. Int J Mol Sci. 2019;20(22).
19. Escartin C, Won SJ, Malgorn C, Auregan G, Berman AE, Chen PC, et al. Nuclear factor erythroid 2-related factor 2 facilitates neuronal glutathione synthesis by upregulating neuronal excitatory amino acid transporter 3 expression. J Neurosci. 2011;31(20):7392-401.
20. French HM, Reid M, Mamontov P, Simmons RA, Grinspan JB. Oxidative stress disrupts oligodendrocyte maturation. J Neurosci Res. 2009;87(14):3076-87.
21. Radhakrishnan S. Cellular redox regulation by the neuronal glutamate and cysteine transporter, EAAT3. Federation of American Societies for Experimental Biology. 2022;36(S1).
22. Cao L, Li L, Zuo Z. N-acetylcysteine reverses existing cognitive impairment and increased oxidative stress in glutamate transporter type 3 deficient mice. Neuroscience. 2012;220:85-9.
23. Berman AE, Chan WY, Brennan AM, Reyes RC, Adler BL, Suh SW, et al. N-acetylcysteine prevents loss of dopaminergic neurons in the EAAC1-/- mouse. Ann Neurol. 2011;69(3):509-20.
24. Aoyama K, Suh SW, Hamby AM, Liu J, Chan WY, Chen Y, et al. Neuronal glutathione deficiency and age-dependent neurodegeneration in the EAAC1 deficient mouse. Nat Neurosci. 2006;9(1):119-26.

25. Delgado-Acevedo C, Estay SF, Radke AK, Sengupta A, Escobar AP, Henriquez-Belmar F, et al. Behavioral and synaptic alterations relevant to obsessive-compulsive disorder in mice with increased EAAT3 expression. Neuropsychopharmacology. 2019;44(6):1163-73.
26. Gerits A, Vancraeyenest P, Vreysen S, Laramee ME, Michiels A, Gijsbers R, et al. Serotype-dependent transduction efficiencies of recombinant adeno-associated viral vectors in monkey neocortex. Neurophotonics. 2015;2(3):031209.
27. Peelaerts W, Brito F, Van den Haute C, Barber Janer A, Steiner JA, Brundin P, et al. Widespread, Specific, and Efficient Transgene Expression in Oligodendrocytes After Intracerebral and Intracerebroventricular Delivery of Viral Vectors in Rodent Brain. Hum Gene Ther. 2021;32(11-12):616-27.
28. Haery L, Deverman BE, Matho KS, Cetin A, Woodard K, Cepko C, et al. Adeno-Associated Virus Technologies and Methods for Targeted Neuronal Manipulation. Front Neuroanat. 2019;13:93.
29. Bauer JA, Zamocka M, Majtan J, Bauerova-Hlinkova V. Glucose Oxidase, an Enzyme "Ferrari": Its Structure, Function, Production and Properties in the Light of Various Industrial and Biotechnological Applications. Biomolecules. 2022;12(3).
30. Eykens C, Rossaert E, Duque S, Rue L, Bento-Abreu A, Hersmus N, et al. AAV9-mediated gene delivery of MCT1 to oligodendrocytes does not provide a therapeutic benefit in a mouse model of ALS. Mol Ther Methods Clin Dev. 2021;20:508-19.
31. Van Vliet KM, Blouin V, Brument N, Agbandje-McKenna M, Snyder RO. The role of the adeno-associated virus capsid in gene transfer. Methods Mol Biol. 2008;437:51-91.
32. Broekman ML, Comer LA, Hyman BT, Sena-Esteves M. Adeno-associated virus vectors serotyped with AAV8 capsid are more efficient than AAV-1 or -2 serotypes for widespread gene delivery to the neonatal mouse brain. Neuroscience. 2006;138(2):501-10.
33. Peelaerts W. Widespread, Specific, and Efficient Transgene Expression in Oligodendrocytes After Intracerebral and Intracerebroventricular Delivery of Viral Vectors in Rodent Brain. Mary Ann Liebert Inc. 2021;32(11-12).
34. Bin JM, Harris SN, Kennedy TE. The oligodendrocyte-specific antibody 'CC1' binds Quaking 7. J Neurochem. 2016;139(2):181-6.
35. Kim SW, Roh J, Park CS. Immunohistochemistry for Pathologists: Protocols, Pitfalls, and Tips. J Pathol Transl Med. 2016;50(6):411-8.
36. Scientific F. PDGFR alpha Goat anti-Mouse, Polyclonal, R&D Systems™.
37. Moore RA, Schmitt BD. Conjunctivitis in children. A refresher survey of diagnosis and contemporary treatment. Clin Pediatr (Phila). 1979;18(1):26-30, 2.
38. Miyamoto N, Pham LD, Hayakawa K, Matsuzaki T, Seo JH, Magnain C, et al. Age-related decline in oligodendrogenesis retards white matter repair in mice. Stroke. 2013;44(9):2573-8.
39. Hong SY, Gil HW, Yang JO, Lee EY, Kim HK, Kim SH, et al. Pharmacokinetics of glutathione and its metabolites in normal subjects. J Korean Med Sci. 2005;20(5):721-6.
40. Malik AR, Szydlowska K, Nizinska K, Asaro A, van Vliet EA, Popp O, et al. SorCS2 Controls Functional Expression of Amino Acid Transporter EAAT3 and Protects Neurons from Oxidative Stress and Epilepsy-Induced Pathology. Cell Rep. 2019;26(10):2792-804 e6.
41. Won SJ, Kim JE, Cittolin-Santos GF, Swanson RA. Assessment at the single-cell level identifies neuronal glutathione depletion as both a cause and effect of ischemia-reperfusion oxidative stress. J Neurosci. 2015;35(18):7143-52.
42. Miller VM, Lawrence DA, Mondal TK, Seegal RF. Reduced glutathione is highly expressed in white matter and neurons in the unperturbed mouse brain--implications for oxidative stress associated with neurodegeneration. Brain Res. 2009;1276:22-30.
43. Dietrich JB, Ribereau-Gayon G, Jung ML, Franz H, Beck JP, Anton R. Identity of the N-terminal sequences of the three A chains of mistletoe (Viscum album L.) lectins: homology with ricin-like plant toxins and single-chain ribosome-inhibiting proteins. Anticancer Drugs. 1992;3(5):507-11.
44. Kaur P, Aschner M, Syversen T. Glutathione modulation influences methyl mercury induced neurotoxicity in primary cell cultures of neurons and astrocytes. Neurotoxicology. 2006;27(4):492-500.
45. van der Ven AJ, Mier P, Peters WH, Dolstra H, van Erp PE, Koopmans PP, et al. Monochlorobimane does not selectively label glutathione in peripheral blood mononuclear cells. Anal Biochem. 1994;217(1):41-7.

46. Ishkaeva RA, Zoughaib M, Laikov AV, Angelova PR, Abdullin TI. Probing Cell Redox State and Glutathione-Modulating Factors Using a Monochlorobimane-Based Microplate Assay. Antioxidants (Basel). 2022;11(2).
47. De Kleijn KMA, Zuure WA, Peijnenborg J, Heuvelmans JM, Martens GJM. Reappraisal of Human HOG and MO3.13 Cell Lines as a Model to Study Oligodendrocyte Functioning. Cells. 2019;8(9).
48. Long PM, Tighe SW, Driscoll HE, Moffett JR, Namboodiri AM, Viapiano MS, et al. Acetate supplementation induces growth arrest of NG2/PDGFRalpha-positive oligodendroglioma-derived tumor-initiating cells. PLoS One. 2013;8(11):e80714.
49. Tiane A. From methylation to myelination: epigenomic and transcriptomic profiling of chronic inactive demyelinated multiple sclerosis lesions. bioRxiv. 2023.
50. Marenna S, Huang SC, Castoldi V, d'Isa R, Costa GD, Comi G, et al. Functional evolution of visual involvement in experimental auto-immune encephalomyelitis. Mult Scler J Exp Transl Clin. 2020;6(4):2055217320963474.
51. Castoldi V, Marenna S, d'Isa R, Huang SC, De Battista D, Chirizzi C, et al. Non-invasive visual evoked potentials to assess optic nerve involvement in the dark agouti rat model of experimental auto-immune encephalomyelitis induced by myelin oligodendrocyte glycoprotein. Brain Pathol. 2020;30(1):137-50.
52. Farley BJ, Morozova E, Dion J, Wang B, Harvey BD, Gianni D, et al. Evoked potentials as a translatable biomarker to track functional remyelination. Mol Cell Neurosci. 2019;99:103393.
53. Marenna S, Huang SC, Dalla Costa G, d'Isa R, Castoldi V, Rossi E, et al. Visual Evoked Potentials to Monitor Myelin Cuprizone-Induced Functional Changes. Front Neurosci. 2022;16:820155.
54. Wu P, Bjorn-Yoshimoto WE, Staudt M, Jensen AA, Bunch L. Identification and Structure-Activity Relationship Study of Imidazo[1,2-a]pyridine-3-amines as First Selective Inhibitors of Excitatory Amino Acid Transporter Subtype 3 (EAAT3). ACS Chem Neurosci. 2019;10(10):4414-29.
55. Ohgoh M, Hanada T, Smith T, Hashimoto T, Ueno M, Yamanishi Y, et al. Altered expression of glutamate transporters in experimental auto-immune encephalomyelitis. J Neuroimmunol. 2002;125(1-2):170-8.
56. Laboratories H. EAE Induction by Active Immunization in C57BL/6 Mice [Available from: https://hookelabs.com/protocols/eaeAI_C57BL6.html#Troubleshooting.
57. Murugesan N, Paul D, Lemire Y, Shrestha B, Ge S, Pachter JS. Active induction of experimental auto-immune encephalomyelitis by MOG35-55 peptide immunization is associated with differential responses in separate compartments of the choroid plexus. Fluids Barriers CNS. 2012;9(1):15.

Acknowledgements – BO is grateful for a postdoctoral scholarship from the Research Foundation Flanders (FWO Vlaanderen). MS is thanked for providing access to the confocal microscope. Rewind Therapeutics and MS are thanked for providing access to the visual evoked potential equipment. KW is thanked for assistance with the stereotaxic frame (Kopf Instruments, CA, USA). MS and LvV are thanked for assistance with confocal microscopy. SV is thanked for providing reagents and assisting in experiments. TV, LvV, MS, AT, BR, EW, SC, DD, PK are thanked for providing assistance, guidance, advice, support and knowledge. FM and LK are thanked for providing assistance in experiments and mental support. Research was funded by grants from the BOF KU Leuven, FWO, and EU (FP7 CHAARM).

Author contributions – LvV and TV conceived and designed the research. BO and LvV performed experiments and data analysis. LvV provided assistance with Leica CM 3050S cryostat and Leica DM400 B LED microscope. BO wrote the paper. All authors carefully edited the manuscript.

SUPPLEMENTARY FIGURES

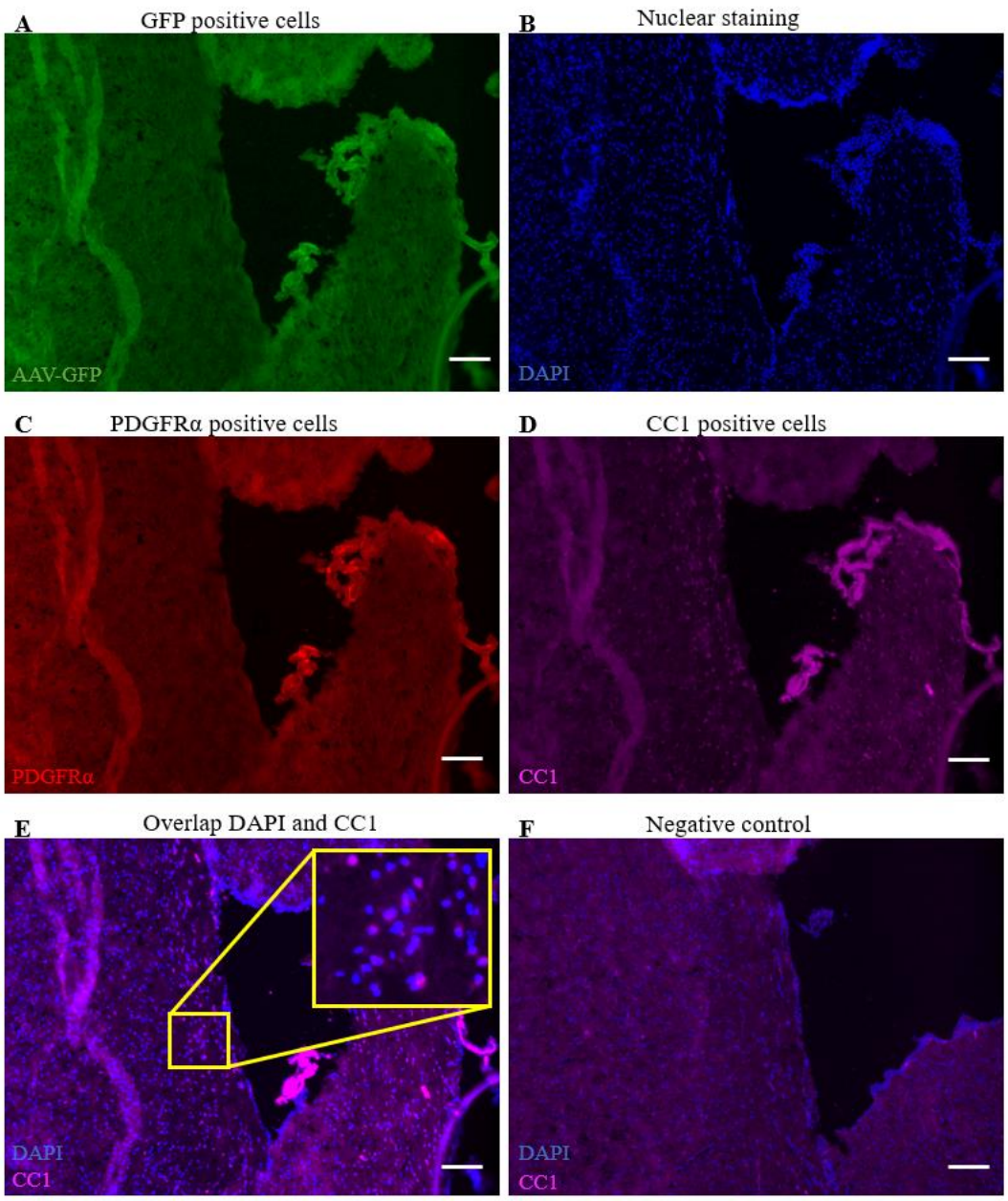

Fig. S1 – **Visualization of CC1 but not PDGFRα in mouse brain tissue without heat induced antigen retrieval and blocking with 10% DAKO protein block. (A-D)** Immunofluorescent staining of the CC using GFP, DAPI, PDGFRα (1/500, R&D systems) and CC1 (Calbiochem). GFP signal from AAVs are not visible since they have faded over time. **(E)** Overlap of DAPI and CC1 staining of the CC with 40x magnification (yellow box). **(F)** Negative control. CC: corpus callosum, CC1: anti-adenomatous polyposis coli clone 1, GFP: green fluorescent protein, PDGFRα: platelet-derived growth factor receptor alpha. (Magnification; 10x, Scalebar; 100 µm)

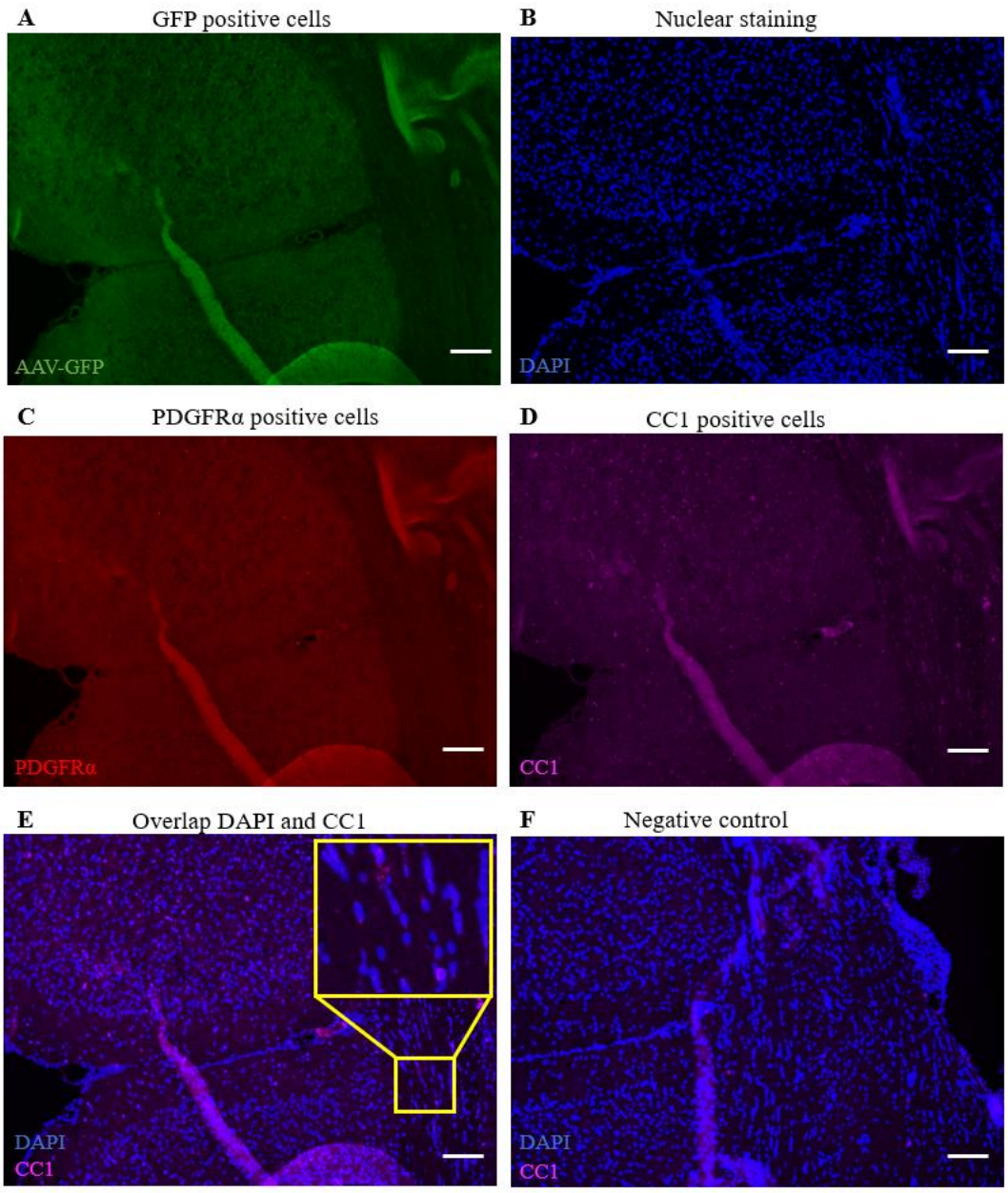

Fig. S2 – **Visualization of CC1 but not PDGFRα in mouse brain tissue after heat-induced antigen retrieval and blocking with 10% DAKO protein block. (A-D)** Immunofluorescent staining of the CC using GFP, DAPI, PDGFRα (1/200, R&D systems) and CC1 (Calbiochem). GFP signal from AAVs are not visible since they have faded over time. **(E)** Overlap of DAPI and CC1 staining of the CC with 40x magnification (yellow box). **(F)** Negative control. CC: corpus callosum, CC1: anti-adenomatous polyposis coli clone 1, GFP: green fluorescent protein, PDGFRα: platelet-derived growth factor receptor alpha. (Magnification; 10x, Scalebar; 100 µm)

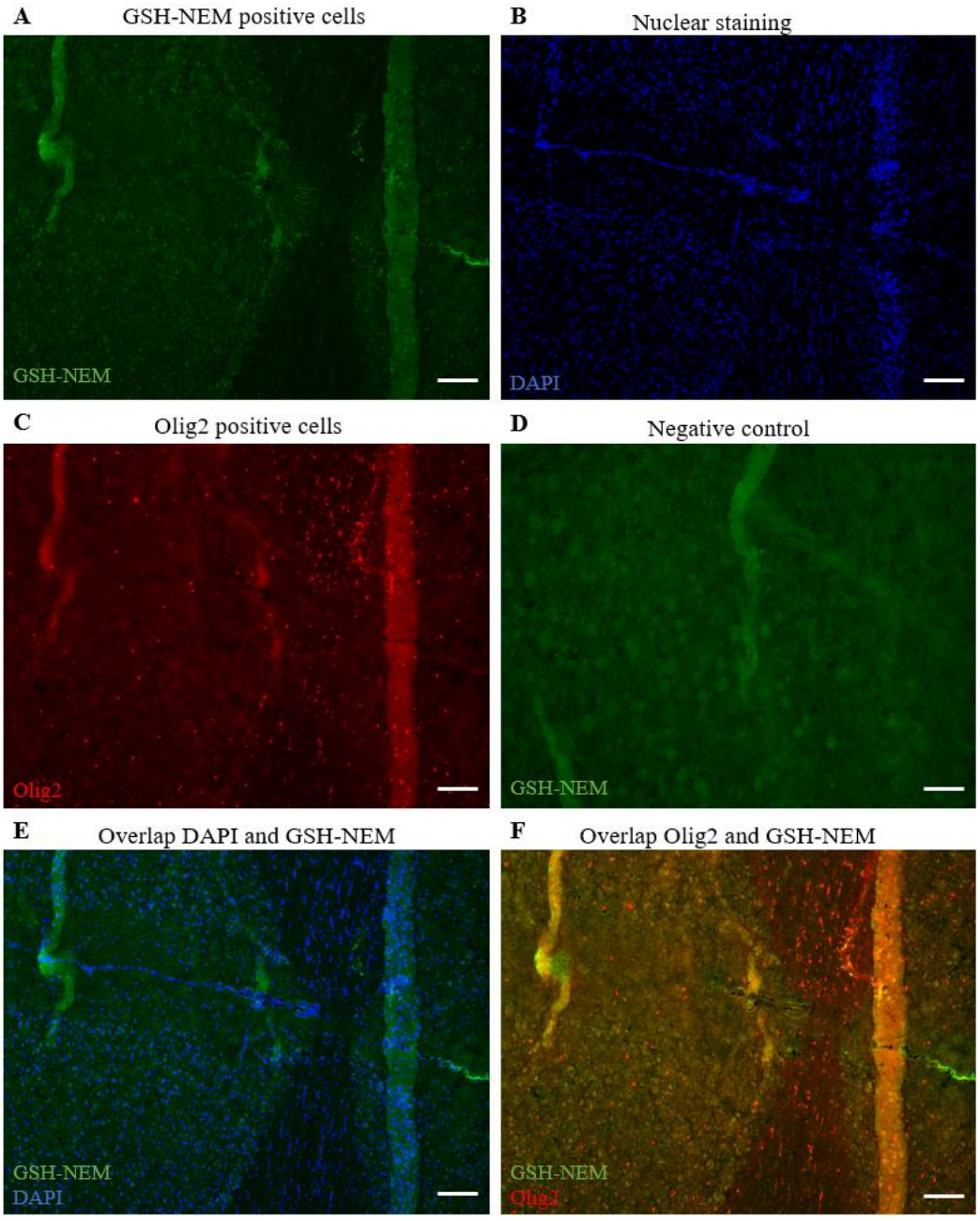

Fig. S3 – **Visualization of GSH-NEM in mouse brain tissue after blocking with 10% DAKO protein block and 4 hours of NEM incubation. (A-C)** Immunofluorescent staining of mouse brain tissue (CC) using GSH-NEM, DAPI and Olig2. **(D)** Negative control. **(E)** Overlap of GSH-NEM and DAPI. **(F)** Overlap of GSH-NEM and Olig2. CC: corpus callosum, GSH-NEM: glutathione-N-ethylmaleimide, NEM: N-ethylmaleimide, Olig2: Oligodendrocyte transcription factor 2. (Magnification; 10x, Scalebar; 100 µm)

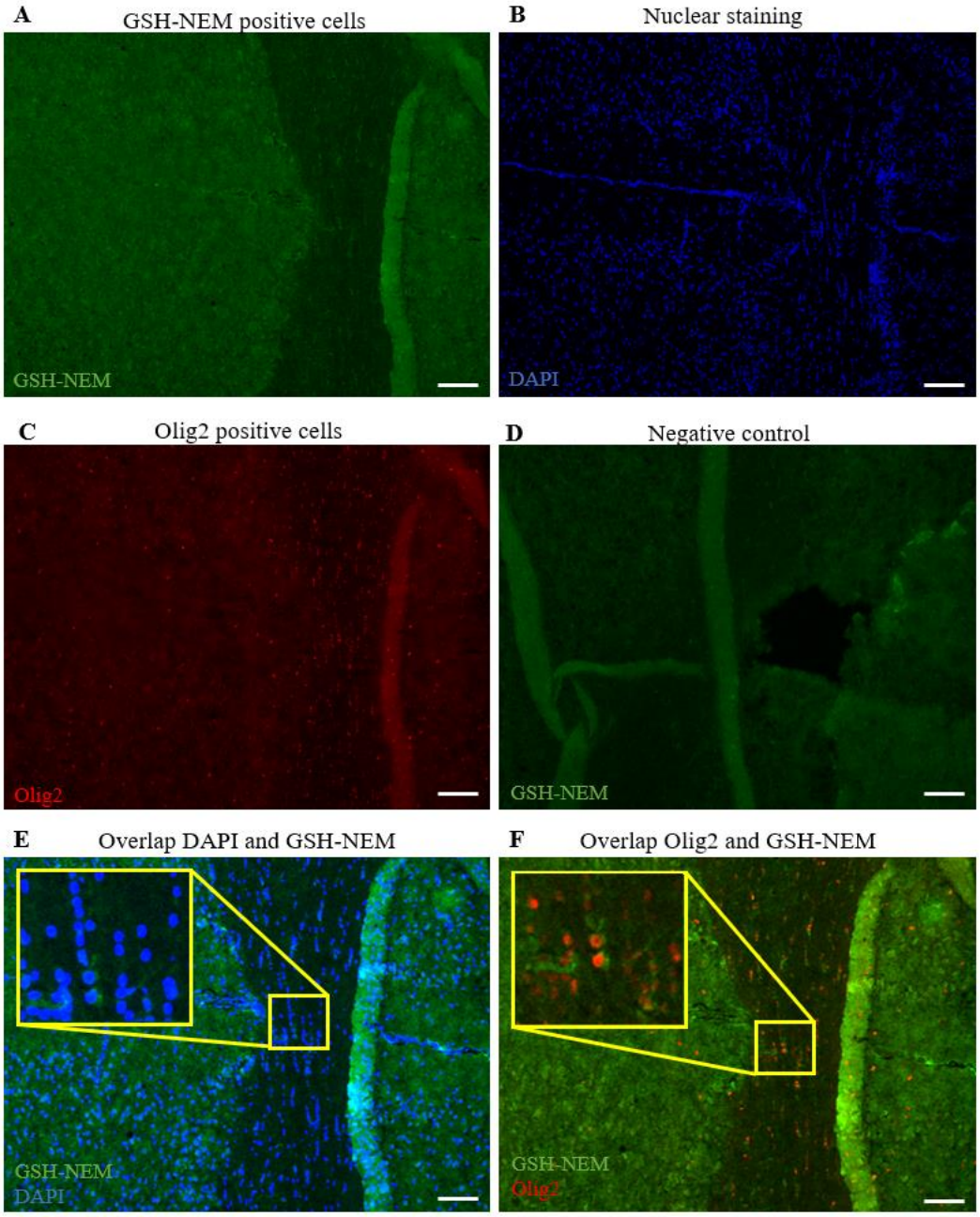

Fig. S4 – **Visualization of GSH-NEM in mouse brain tissue after blocking with 10% DAKO protein block and 1 hour of NEM incubation. (A-C)** Immunofluorescent staining of mouse brain tissue (CC) using GSH-NEM, DAPI and Olig2. **(D)** Negative control. **(E)** Overlap of GSH-NEM and DAPI of the CC with 40x magnification (yellow box). **(F)** Overlap of GSH-NEM and Olig2 of the CC with 40x magnification (yellow box). CC: corpus callosum, GSH-NEM: glutathione-N-ethylmaleimide, NEM: N-ethylmaleimide, Olig2: Oligodendrocyte transcription factor 2. (Magnification; 10x, Scalebar; 100 µm)

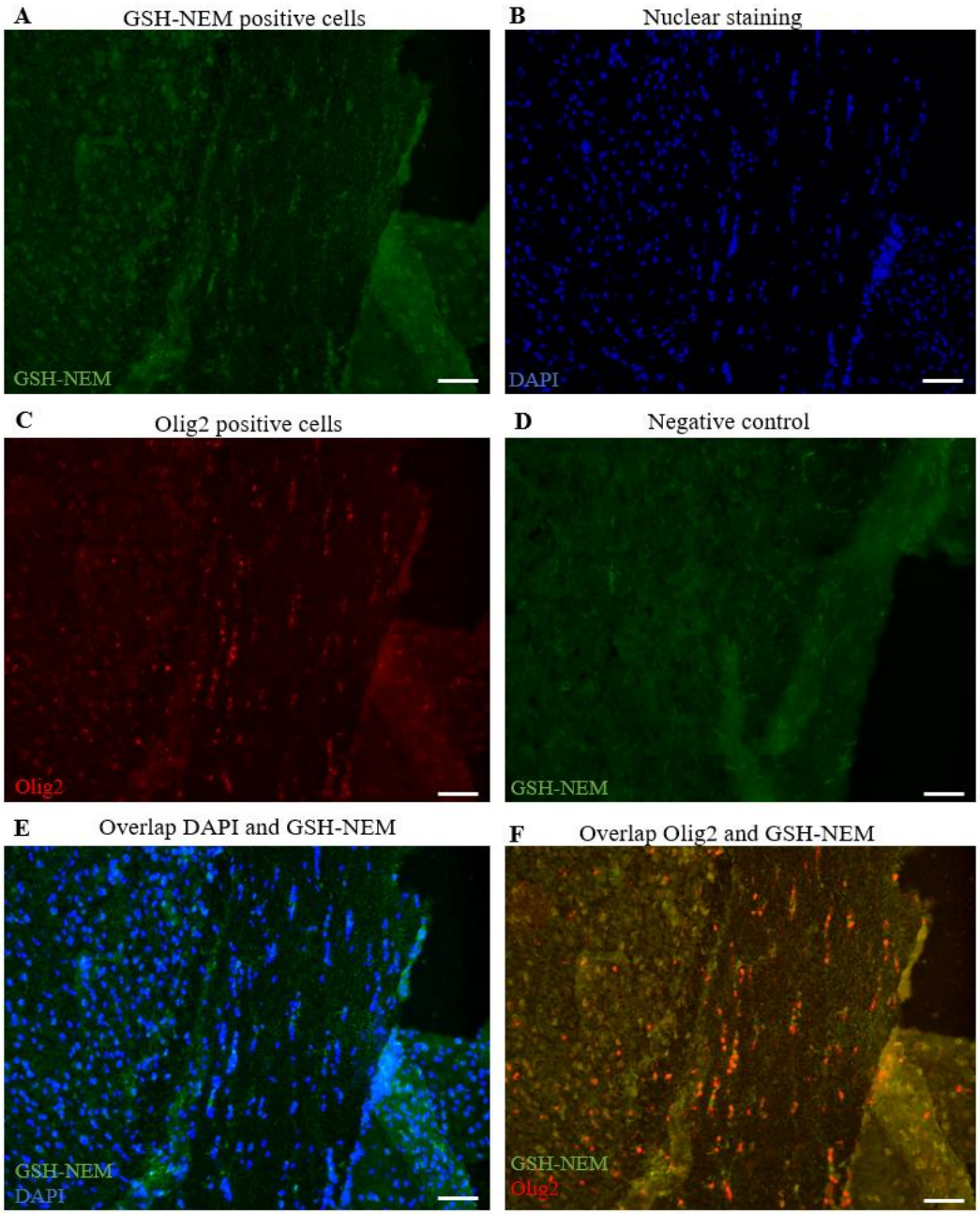

Fig. S5 – **Visualization of GSH-NEM in mouse brain tissue after blocking with 10% normal donkey and normal rabbit serum, Sudan black and 4 hours of NEM incubation. (A-C)** Immunofluorescent staining of mouse brain tissue (CC) using GSH-NEM, DAPI and Olig2. **(D)** Negative control. **(E)** Overlap of GSH-NEM and DAPI. **(F)** Overlap of GSH-NEM and Olig2. CC: corpus callosum, GSH-NEM: glutathione-N-ethylmaleimide, NEM: N-ethylmaleimide, Olig2: Oligodendrocyte transcription factor 2. (Magnification; 10x, Scalebar; 100 µm)

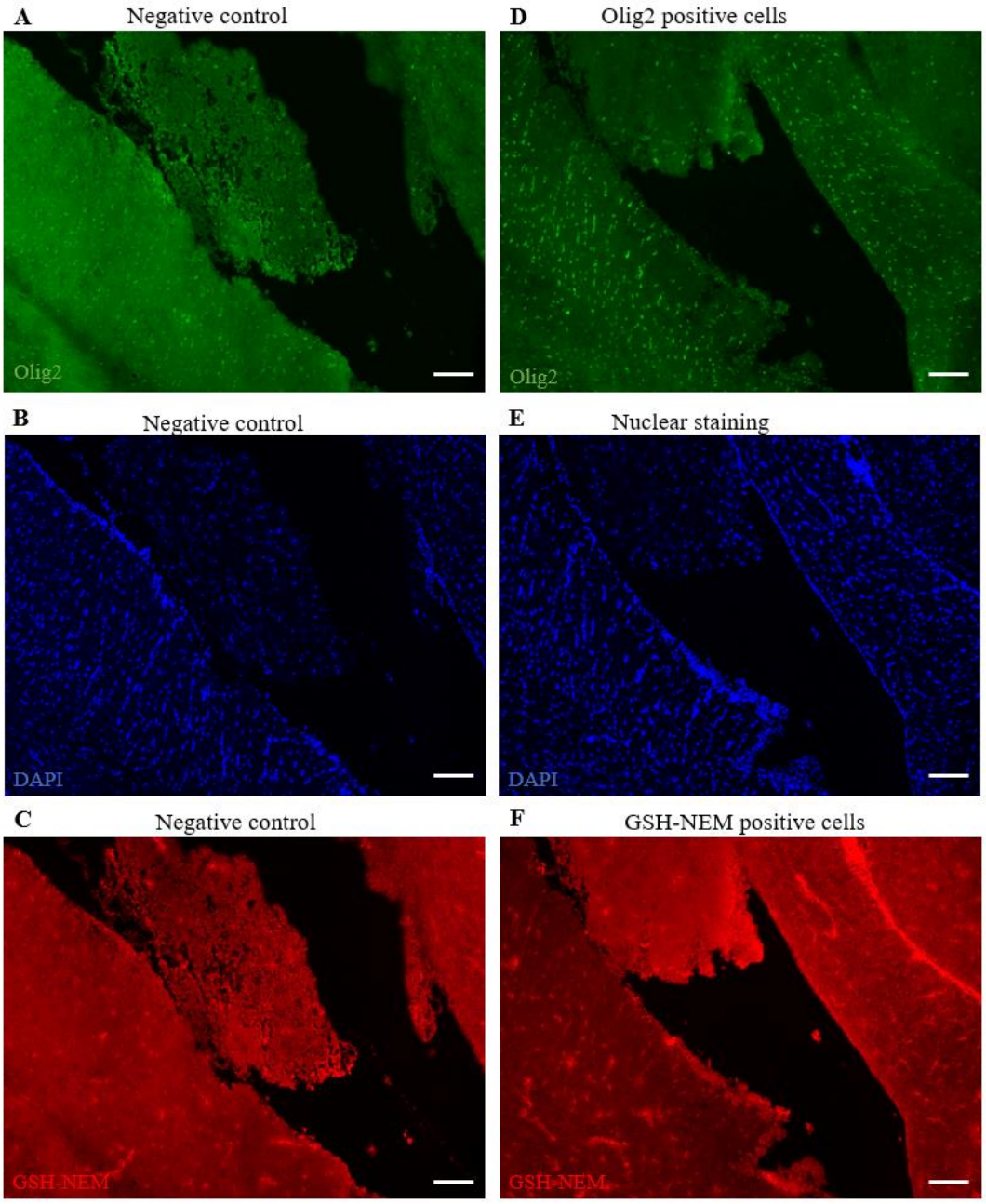

Fig. S6 – **GSH-NEM is not visible in wild-type mouse brain tissue (not fixed in NEM) after blocking with 10% DAKO protein block and 4 hours of NEM incubation. (A-C)** Negative control. **(D-F)** Immunofluorescent staining of wild-type mouse brain tissue (CC) using GSH-NEM, DAPI and Olig2. CC: corpus callosum, GSH-NEM: glutathione-N-ethylmaleimide, NEM: N-ethylmaleimide, Olig2: Oligodendrocyte transcription factor 2. (Magnification; 10x, Scalebar; 100 µm)

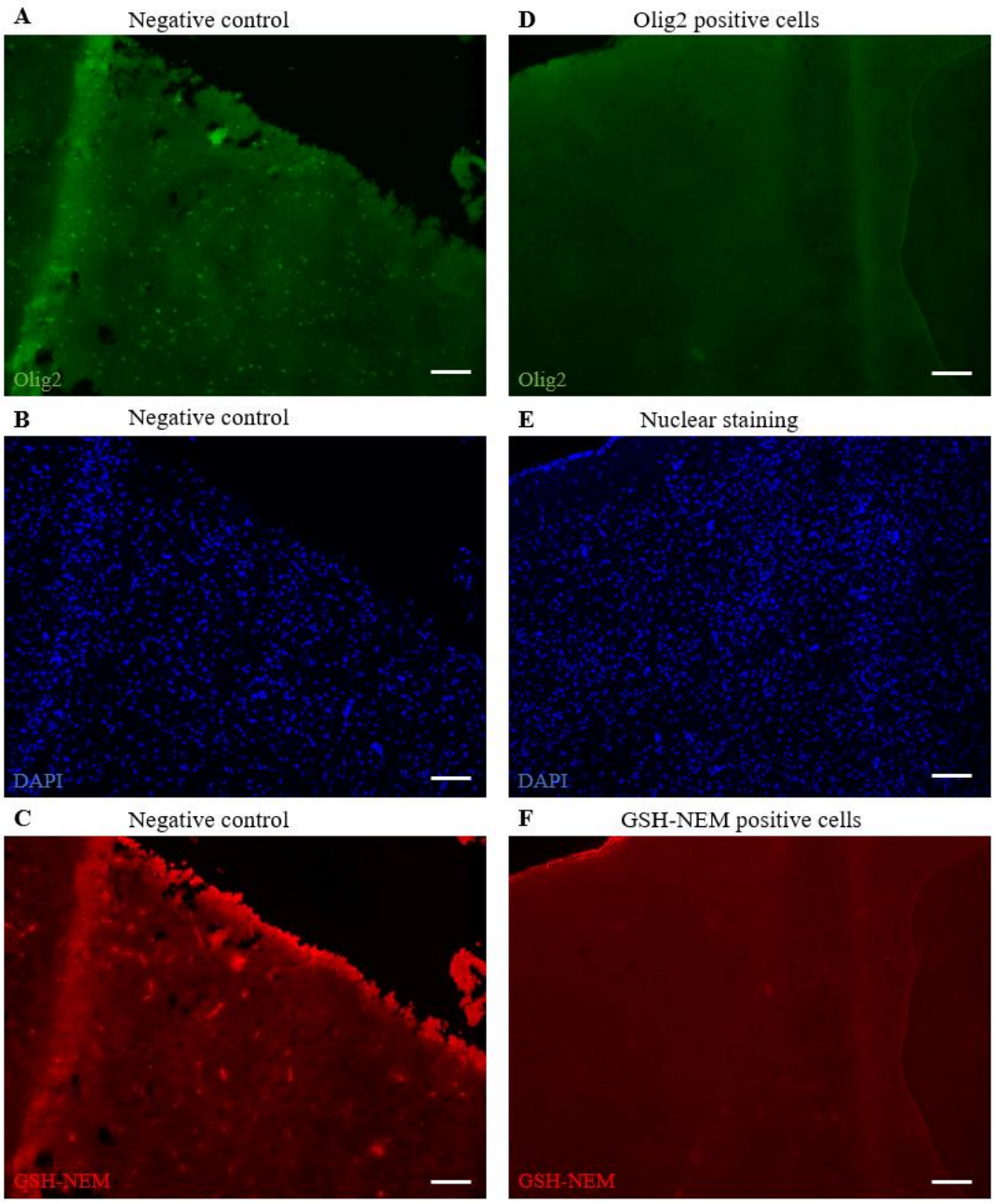

Fig. S7 – **GSH-NEM is not visible in EAE mouse brain tissue (not fixed in NEM) after blocking with 10% DAKO protein block and 4 hours of NEM incubation. (A-C)** Negative control. **(D-F)** Immunofluorescent staining of EAE mouse brain tissue (CC) using GSH-NEM, DAPI and Olig2. CC: corpus callosum, GSH-NEM: glutathione-N-ethylmaleimide, NEM: N-ethylmaleimide, Olig2: Oligodendrocyte transcription factor 2. (Magnification; 10x, Scalebar; 100 µm)

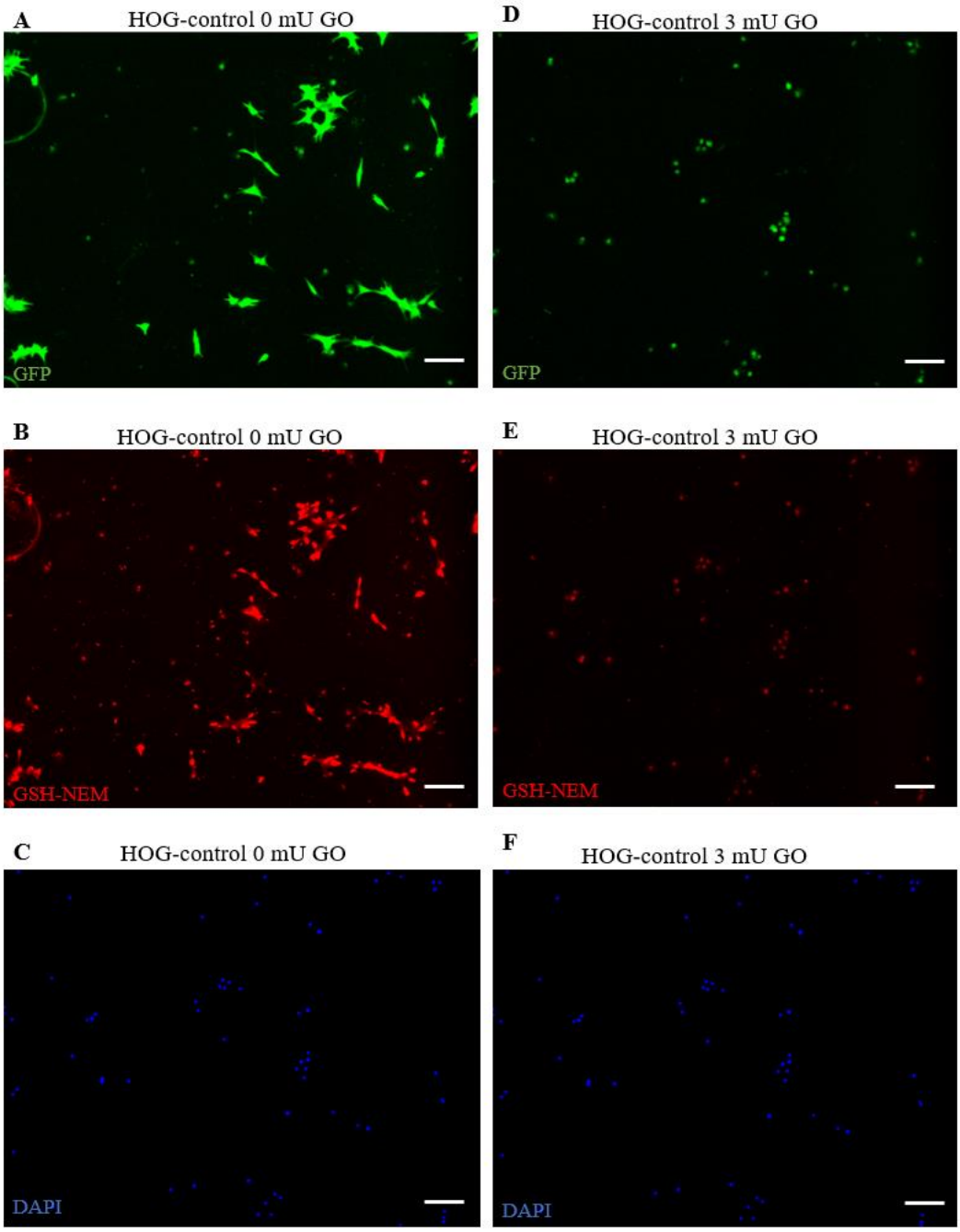

Fig. S8 – **HOG-control cells treated with 0 mU GO show more differentiation and GSH production than HOG-control cells treated with 3 mU GO. (A-C)** HOG-control cells treated with 0 mU GO with GFP signal, GSH-NEM staining and DAPI counterstaining**. (D-F)** HOG-control cells treated with 3 mU GO with GFP signal, GSH-NEM staining and DAPI counterstaining. GFP: green fluorescent protein, GO: glucose oxidase, GSH-NEM: glutathione-N-ethylmaleimide, NEM: N-ethylmaleimide. (Magnification; 10x, Scalebar; 100 µm)

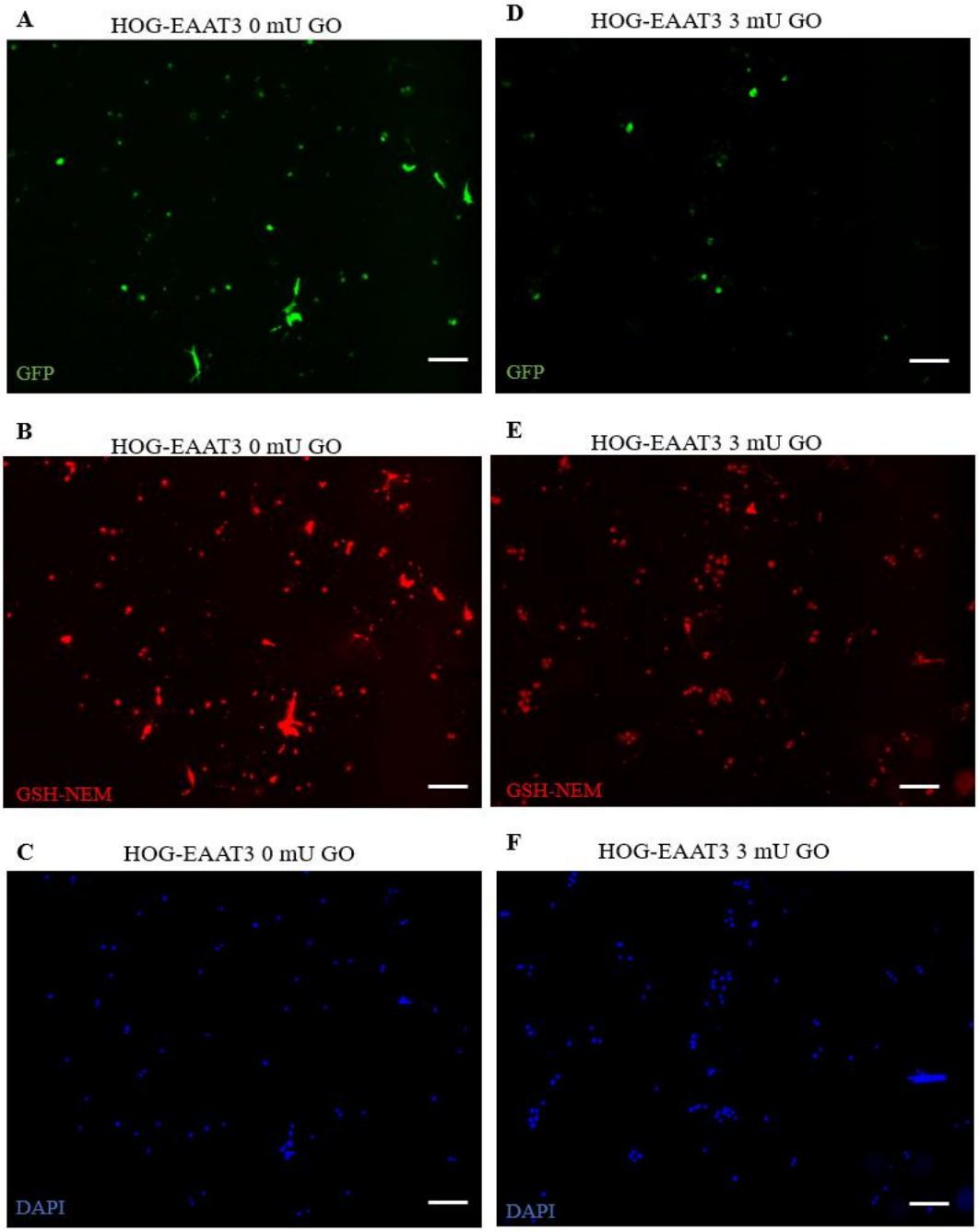

Fig. S9 – **HOG-EAAT3 overexpressing cells treated with 0 mU GO show more differentiation and GSH production than HOG-EAAT3 cells treated with 3 mU GO. (A-C)** HOG-EAAT3 cells treated with 0 mU GO with GFP signal, GSH-NEM staining and DAPI counterstaining. **(D-F)** HOG-EAAT3 cells treated with 3 mU GO with GFP signal, GSH-NEM staining and DAPI counterstaining. EAAT3: excitatory amino acid transporter 3, GFP: green fluorescent protein, GO: glucose oxidase, GSH-NEM: glutathione-N-ethylmaleimide, NEM: N-ethylmaleimide. (Magnification; 10x, Scalebar; 100 µm)

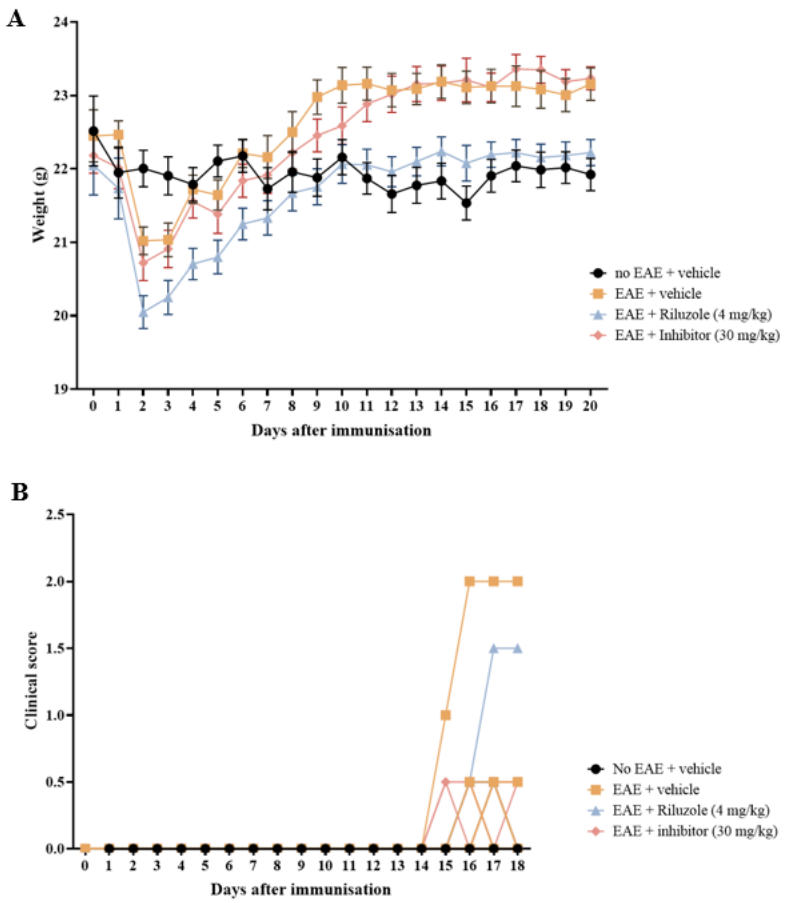

Fig. S10 – **EAAT3 inhibitor increases average mice weight and does not affect clinical scores.** All mice were weighted and scored once every day for 20 days. **(A)** Monitored average weights of mice after immunization and treatment (n=18/group). **(B)** Average clinical scores of EAE mice after immunization and treatment (n=18/group). EAE: experimental auto-immune encephalomyelitis. VEP: visual evoked potentials.

SUPPLEMENTARY EXPERIMENTAL PROCEDURES

AAV in vivo and post-mortem

Mouse model

Sox10Cre mice and C57BL/6 wild-type mice of around 8-20 weeks old were purchased from Jackson Laboratories (ME, USA). Mice were housed under a 12h light/dark cycle, at a temperature of around 21-24°C and had free access to food and water. All animal experiments were carried out in accordance with the European Communities Council Directive of 2010 (2010/63EU) and approved by the Ethical Committee for Animal Experimentation (ECAE) of Hasselt University (Limburg, Belgium).

Stereotactic AAV injections and Tamoxifen treatment

AAV with serotype 2.8 (MAG2.2-intron-eGFP) and AAV with serotype 2.9 (MAG2.2-intron-eGFP) were purchased from Leuven Viral Vector Core. All mice received a subcutaneous injection of Temgesic® injection (Eumedica, Manage, Belgium) as a painkiller and were anesthetized with isoflurane for both induction and maintenance of anesthesia. Mice were then placed onto a stereotaxic frame (Kopf Instruments, CA, USA). Stereotactic injections of the AAVs (2µl) were performed bilaterally intracerebroventricularly (AP -1mm; ML +1.6 mm; DV -2 mm and AP -1 mm; ML -1.6mm; ML -2mm, relative to bregma) or in the corpus callosum (AP -1mm; ML 0 mm; DV -1,8mm, relative to bregma) of 8-20 weeks old mice, using a 2 µl Hamilton syringe at a rate of 0.5 µl/min. The needle was kept in place for an additional 2 minutes after injection and withdrawn slowly. Following surgery, the animals were monitored until they recovered from the anesthesia and were housed per 2. Six days after surgery, mice received one intraperitoneal Tamoxifen injection of 5 µl/g (T5648, Sigma-Aldrich, MO, USA) during 3 days. Mice were sacrificed 7 days after the last Tamoxifen injection.

Tissue sample preparation

Animals were sacrificed at 7 days after the last Tamoxifen injection by a lethal Dolethal injection (200 mg/kg, Vetoquinol, Northamptonshire, UK), followed by a transcardial perfusion. Brains were collected from each animal and immersed in 4% paraformaldehyde (PFA, P6148, Sigma-Aldrich, MO, USA) overnight. Afterwards, brains were incubated in a sucrose gradient (10%, 20% and 30%, each overnight) for cryoprotection. Afterwards brains were snap-frozen in liquid nitrogen and embedded in Tissue-Tek optimal cutting temperature compound (VWR, Leuven, Belgium). Brains were cut in coronal plane with a Leica CM 3050S cryostat (Wetzlar, Germany) to obtain 10 µm sections. Brain sections were mounted per three on glass slides and stored at -20°C until used.

Fluorescent immunohistochemistry

Frozen coronal brain sections were generated via cryosectioning (Leica, Wetzlar, Germany) at 10 µm thickness and were stained for platelet-derived growth factor receptor alpha (PDGFRα) and anti-adenomatous polyposis coli clone CC1 (APC). Cryosections were dried and incubated in acetone for 10 minutes and washed with 0,05% PBS-Tween. To perform heat-induced antigen retrieval, sections were placed in boiling citrate buffer at room temperature for 10 minutes. Afterwards, sections were washed with 0,05% PBS-Tween. Non-specific background signal was blocked by incubating cryosections for 30 minutes in 10% diluted protein block (Dako, Glostrup, Denmark) or 10% normal donkey serum (NDS, Milipore, MA USA) and 10% normal goat serum (NGS, Milipore, MA, USA) in PBS. After blocking, cryosections were incubated overnight at 4°C with goat anti-mPDGFRα (1/200, R&D systems, MN, USA) and mouse anti-APC (anti-Ab-7 or anti-CC1, 1/50, Calbiochem, CA, USA). Unattached primary antibodies were washed off with PBS and incubated for 1 hour at room temperature with secondary antibodies Alexafluor 647 goat anti-mouse IgG (1/600, Invitrogen, MA, USA) and Alexafluor 555 donkey anti-goat IgG (1/600, Invitrogen, MA, USA). Counterstaining of nuclei was done with DAPI (Invitrogen, MA, USA) for 10 minutes at room temperature. Cryosections were washed with PBS and mounted with fluorescent mounting medium (DAKO, Glostrup, Denmark). Images of the corpus callosum and left/right ventricles were taken using the Leica DM400 B LED microscope (Wetzlar, Germany) and visualized with the Fiji ImageJ software. Details of primary antibodies are shown in Table S1.

HOG cells

Lentiviral transduction

The lentiviral vector (pCHMWS-MmEAAT3-T2A-eGFP-Ires-Puro), which expresses EAAT3, GFP and a puromycin resistance gene was used to transduce HOG cells to gain a stable overexpression. Additionally, the lentiviral vector (pCHMWS-eGFP-T2A-fLuc-Ires-Puro) co-expressing only GFP and puromycin was used as a control. Both lentiviral vectors were purchased from Leuven Viral Vector Core. Puromycin (10 µg/ml, InvivoGen, San Diego, CA, USA) was used to treat the cells 48 hours and 72 hours after transduction to select cells that were successfully transduced with the lentiviral vectors.

Fluorescent immunocytochemistry

HOG cells transduced with EAAT3 and control virus were seeded at a density of 15 000 cells per well in a PLL coated 24-well plate containing round cover glasses. Next, cells were treated with 0 mU and 3 mU of glucose oxidase at day 0 and 2 to induce oxidative stress. At day 4, cells were fixed with 4% paraformaldehyde (PFA, P6148, Sigma-Aldrich, MO, USA) containing 10 mM N-ethylmaleimide (NEM, Sigma-Aldrich, MO, USA). Blocking was performed by incubation of cells in 1% bovine serum albumin (BSA, Biowest, Nuaillé, France) for 30 minutes at room temperature. Next, cells were incubated in 10 mM NEM in PBS for 1 hour at 4°C. Primary antibodies were diluted in 1% BSA and cells were incubated with mouse anti-GSH-NEM (1/600, MAB3194, clone8.1GSH, Milipore, MA USA) for 3 hours at room temperature. After washing with PBS, cells were incubated for 1 hour in the dark at room temperature or overnight at 4°C with Alexafluor 555 goat anti-mouse IgG H+L (1/600, Invitrogen, MA, USA). Counterstaining of nuclei was done with DAPI (Invitrogen, MA, USA) for 10 minutes. The round glass cover glasses were mounted onto microscope slides with fluorescent mounting medium (DAKO, Glostrup, Denmark). Six random images of each cover glass were taken using the Leica DM400 B LED microscope (Wetzlar, Germany) and visualized with the Fiji ImageJ software.

Quantitative PCR

Total RNA was isolated using the Trizol reagent method as described by Maastricht University. RNA purity and concentration were determined by using a Nanodrop microvolume spectrophotometer (Isogen Life Sciences, Utrecht, The Netherlands). Next, cDNA synthesis was accomplished by using qScript cDNA Supermix (Quanta Biosciences, MA, USA) and iScript cDNA Synthesis Kit (Bio Rad, CA, USA). Quantitative PCR was performed on the QuantStudio 3 Real-Time PCR instrument 96-well 0.1 Block (Applied Biosystems, MA, USA). The total reaction volume of 10 µl contained PowerUp SYBR Green master mix (Applied Biosystems, MA, USA), 10 µM forward and reverse primers (details in Table S2), autoclaved miliQ, and 5 ng cDNA template. The relative quantification of gene expression was completed by using the comparative Ct method with normalization to the most stable reference genes.

Table S1 – Used primary antibodies with supplier and identifier.

Primary antibodies	**Supplier**	**Identifier**
Anti-APC/anti-Ab-7/anti-CC1	Calbiochem	Cat# OP80
Anti-GSH-NEM	Milipore	Cat# MAB3194, clone8.1GSH
Anti-MBP IgG	Milipore	Cat# MAB386
Anti-O4 IgM	R&D systems	Cat# MAB1326
Anti-Olig2	R&D systems	Cat# AF2418

Table S2 – Used forward and reverse primers for quantitative PCR

Housekeeping genes			
Species	**Gene**	**Forward primer**	**Reverse primer**
Human	CYCA	AGA CTG AGT GGT TGG ATG GC	TCG AGT TGT CCA CAG TCA GC
Human	GAPDH	CGC AGT AGA AAT TGT GGC CA-	CCT TGA CAG TGC CCT TGA AC
Human	PGK	CTG GGC AAG GAT GTT CTG TT	GCA TCT TTT CCC TTC CCT TC
Human	YWHAZ	CTT GAC ATT GTG GAC ATC GG	TAT TTG TGG GAC AGC ATG GA
Genes of interest			
Species	**Gene**	**Forward primer**	**Reverse primer**
Human	ID2	ATG AAA GCC TTC AGT CCC GT	CGA TCT GCA GGT CCA AGA TG
Human	MBP	GAT GTG ATG TGA TGG CGT CAC AGA A	GGT TTT CAG CGT CTA GCC AT
Human	SLC1A1	TGA TGA GTT TCA GCA TCC GCA	GGT GGT GCT AAG CAT TAC CA